Article

Cell Host & Microbe

Aryl Hydrocarbon Receptor Modulation by Tuberculosis Drugs Impairs Host Defense and Treatment Outcomes

Graphical Abstract

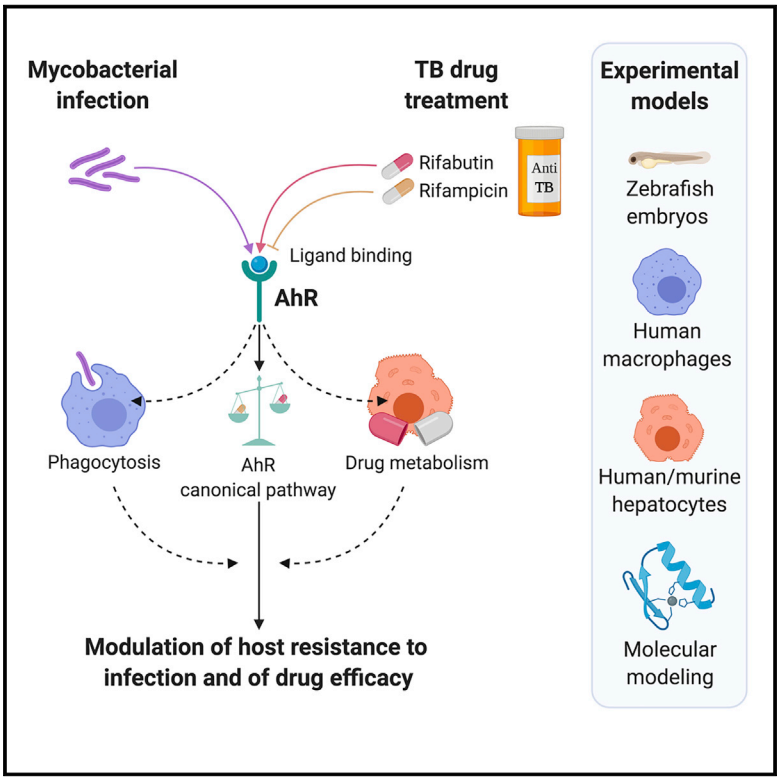

Highlights

- AhR concomitantly senses mycobacterial infection and TB drug treatment
- AhR sensing of TB drugs impairs host defense and increases drug metabolism
- AhR inhibition enhances efficacy of rifabutin in *M. marinum*-infected zebrafish

Authors

Andreas Puyskens, Anne Stinn, Michiel van der Vaart, ..., Annemarie H. Meijer, Stefan H.E. Kaufmann, Pedro Moura-Alves

Correspondence

kaufmann@mpiib-berlin.mpg.de (S.H.E.K.), pedro.mouraalves@ludwig.ox.ac.uk (P.M.-A.)

In Brief

Host-directed therapy is a strategy to improve the lengthy treatment of tuberculosis (TB). Puyskens et al. find that the aryl hydrocarbon receptor (AhR) binds to several TB drugs, resulting in altered host defense and drug metabolism. Modulation of the AhR in infected zebrafish embryos leads to improved treatment efficacy.

Puyskens et al., 2020, Cell Host & Microbe *27*, 238–248
February 12, 2020
https://doi.org/10.1016/j.chom.2019.12.005

CellPress

Aryl Hydrocarbon Receptor Modulation by Tuberculosis Drugs Impairs Host Defense and Treatment Outcomes

Andreas Puyskens,[1] Anne Stinn,[1,2] Michiel van der Vaart,[3] Annika Kreuchwig,[4] Jonas Protze,[4] Gang Pei,[5] Marion Klemm,[1] Ute Guhlich-Bornhof,[1] Robert Hurwitz,[6] Gopinath Krishnamoorthy,[1] Marcel Schaaf,[3] Gerd Krause,[4] Annemarie H. Meijer,[3] Stefan H.E. Kaufmann,[1,7,9,*] and Pedro Moura-Alves[1,8,9,10,*]

[1]Department of Immunology, Max Planck Institute for Infection Biology, Charitéplatz 1, Berlin 10117, Germany
[2]Department for Structural Infection Biology, Center for Structural Systems Biology, Notkestraße 85, Hamburg 22607, Germany
[3]Institute of Biology, Leiden University, Sylviusweg 72, Leiden 2333, the Netherlands
[4]Leibniz-Forschungsinstitut für Molekulare Pharmakologie, Robert-Rössle-Strasse 10, Berlin 13125, Germany
[5]Institute of Immunology, Friedrich Loeffler Institute, Südufer 10, Greifswald-Insel Riems 17493, Germany
[6]Protein Purification Core Facility, Max Planck Institute for Infection Biology, Charitéplatz 1, Berlin 10117, Germany
[7]Hagler Institute for Advanced Study at Texas A&M University, College Station, TX 77843, USA
[8]Ludwig Institute for Cancer Research, Nuffield Department of Clinical Medicine, University of Oxford, Oxford OX3 7DQ, UK
[9]Senior author
[10]Lead Contact
*Correspondence: kaufmann@mpiib-berlin.mpg.de (S.H.E.K.), pedro.mouraalves@ludwig.ox.ac.uk (P.M.-A.)
https://doi.org/10.1016/j.chom.2019.12.005

SUMMARY

Antimicrobial resistance in tuberculosis (TB) is a public health threat of global dimension, worsened by increasing drug resistance. Host-directed therapy (HDT) is an emerging concept currently explored as an adjunct therapeutic strategy for TB. One potential host target is the ligand-activated transcription factor aryl hydrocarbon receptor (AhR), which binds TB virulence factors and controls antibacterial responses. Here, we demonstrate that in the context of therapy, the AhR binds several TB drugs, including front line drugs rifampicin (RIF) and rifabutin (RFB), resulting in altered host defense and drug metabolism. AhR sensing of TB drugs modulates host defense mechanisms, notably impairs phagocytosis, and increases TB drug metabolism. Targeting AhR *in vivo* with a small-molecule inhibitor increases RFB-treatment efficacy. Thus, the AhR markedly impacts TB outcome by affecting both host defense and drug metabolism. As a corollary, we propose the AhR as a potential target for HDT in TB in adjunct to canonical chemotherapy.

INTRODUCTION

The aryl hydrocarbon receptor (AhR) is an evolutionary highly conserved ligand-dependent transcription factor that functions as a cellular sensor of both extrinsic and intrinsic chemical signals (Kawajiri and Fujii-Kuriyama, 2017). AhR ligands are diverse and encompass environmental toxins, cell- and microbe-derived metabolites, and dietary products (Hubbard et al., 2015). Ligand binding to the AhR, induces transcription of target genes involved in xenobiotic metabolism, cell homeostasis, embryonic development, and immunity (Gutiérrez-Vázquez and Quintana, 2018). Previously, our group described AhR sensing of the naphthoquinone phthiocol (Pht) produced by *Mycobacterium tuberculosis* (*Mtb*), the causative agent of tuberculosis (TB) in humans, and its importance in host defense against *Mtb* (Moura-Alves et al., 2014). TB remains the leading cause of death by a single infectious agent, and the emergence of antimicrobial resistance (AMR) in TB has led to a public health crisis (World Health Organization, 2019). Non-compliance and incorrect use of TB drugs have contributed to the emergence of multidrug-resistant (MDR) and extensively drug-resistant (XDR) *Mtb* strains, rendering several first-line drugs ineffective. AMR requires prolonged and more expensive chemotherapy regimens, often with severe adverse events for patients and creating an enormous economic burden (World Health Organization, 2019). Host-directed therapy (HDT) is an emerging concept currently explored as adjunct strategy for TB treatment to counteract AMR (Kolloli and Subbian, 2017; Kaufmann et al., 2018). Given that the AhR is positioned at the center of xenobiotic metabolism regulation and host defense, the AhR represents a promising target for HDT in TB. Here, we explore whether AhR not only modulates infection (Moura-Alves et al., 2014) but also drug therapy. We demonstrate that (1) the AhR binds and senses several first- and second-line TB drugs, (2) AhR modulation by TB drugs inhibits macrophage phagocytosis, (3) the AhR is involved in the metabolism of rifabutin (RFB), and (4) inhibition of the AhR by a specific small-molecule inhibitor enhances RFB-mediated antimicrobial activity. Thus, we propose the AhR as a candidate target for future HDT in adjunct to canonical TB drug treatment.

RESULTS

TB Drugs Modulate AhR Signaling

Using a previously established macrophage AhR luciferase reporter system (THP-1 AhR reporter) (Moura-Alves et al., 2014),

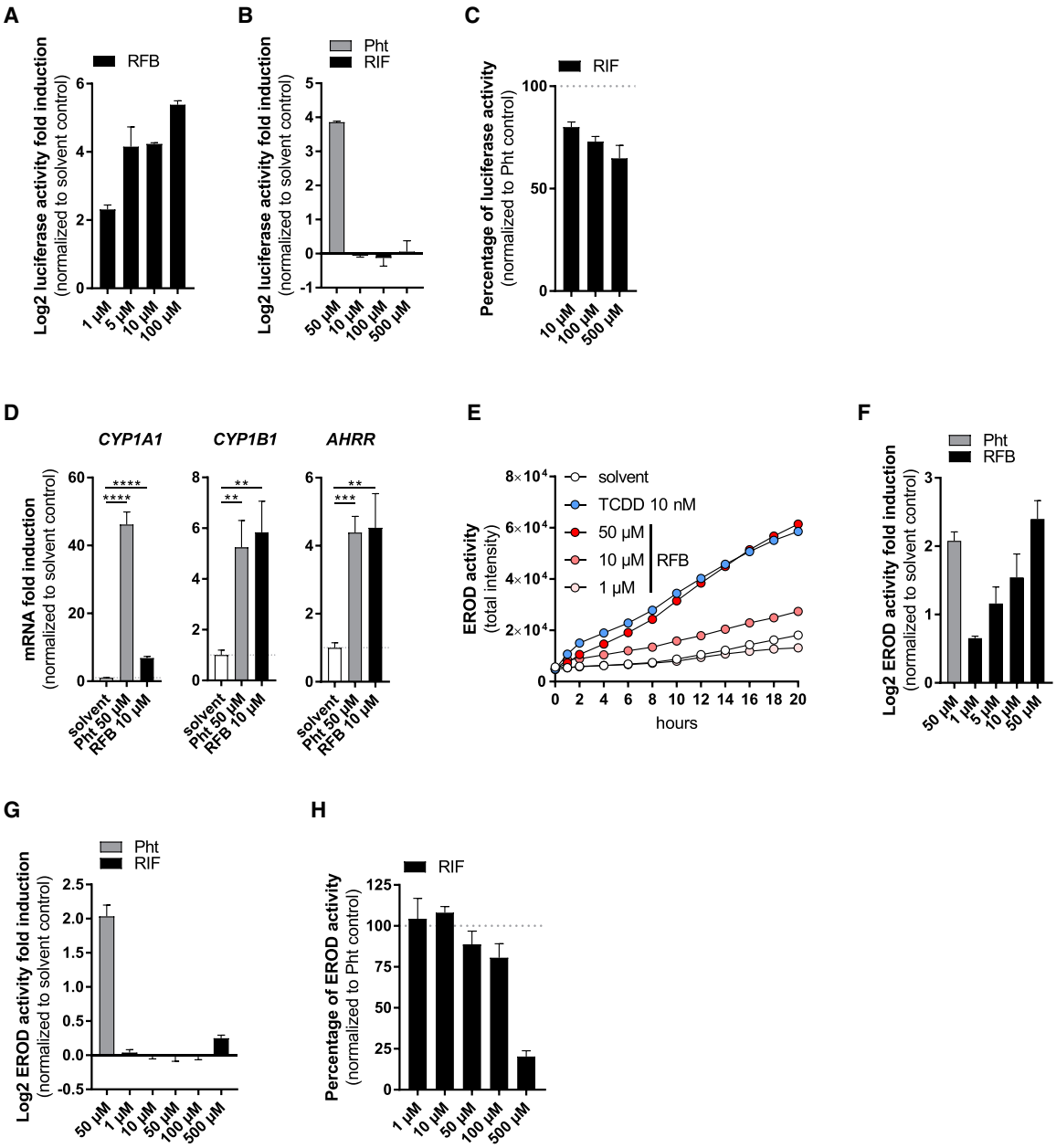

Figure 1. RFB and RIF Modulate AhR Signaling *In Vitro*

(A and B) Luciferase activity of macrophage (THP-1) luciferase AhR reporter cells upon 4 h stimulation with RFB (A) or RIF or Pht (B).

(C) Pht-RIF competition assay: first pre-incubation with increasing concentrations of RIF for 1 h, followed by 3 h stimulation together with 50 μM Pht or Pht alone as control.

(D) Gene-expression analysis of AhR-dependent genes in THP-1 macrophages upon stimulation with Pht or RFB for 4 h.

(E and F) Hepatic CYP1A1 enzymatic activity (Hepa-1c1c7) upon stimulation with increasing concentrations of RFB and (E) TCDD over time or (F) Pht after 24 h.

(G and H) Hepatic CYP1A1 enzymatic activity (Hepa-1c1c7) upon stimulation with (G) Pht or (H) increasing concentrations of RIF.

(H) Pht-RIF competition assay: first pre-incubation with increasing concentrations of RIF for 1 h, followed by stimulation together with 50 μM Pht or Pht alone for 3 h.

(A–C and F) 1 representative of n = 4 independent experiments.

(D, E, G, and H) 1 representative of n = 3 independent experiments.

(A–D and F–H) Mean ± SD shown.

(D) Unpaired t test.

(E) Mean only shown. $^{**}p \leq 0.01$, $^{***}p \leq 0.001$, $^{****}p \leq 0.0001$.

See also Figure S1 and S2.

Table 1. List of TB Drugs Tested in the AhR Reporter Assay

Drug	Abbreviation	AhR Modulation
Group 1: First-Line Oral TB Drugs		
Ethambutol	EMB	No effect
Isoniazid	INH	No effect
Pyrazinamide	PZA	No effect
Rifabutin	RFB	Activator
Rifampicin	RIF	Inhibitor
Rifapentine	RPT	Inhibitor
Group 2: Injectable TB Drugs		
Amikacin	AMK	No effect
Kanamycin	KAN	No effect
Streptomycin	STM	No effect
Group 3: Fluoroquinolones		
Enrofloxacin	ERF	Inhibitor
Moxifloxacin	MXF	Inhibitor
Group 4: Second-Line Oral TB Drugs		
Bedaquiline	BDQ	Activator
Clofazimine	CFZ	Inhibitor
Ethionamide	ETA	Inhibitor
Linezolid	LZD	Activator
p-Aminosalicyclic acid	PAA	No effect
Group 5: Currently Not Included in Core MDR-TB Regimen		
Thiacetazone	THZ	Inhibitor

we tested diverse TB drugs in clinical use for their potential to modulate AhR signaling. Of note, TB drug concentrations used in our study conform with drug concentrations used in another large European study testing different animal models (PreDiCT-TB) (Kaufmann et al., 2015). Several TB drugs modulated AhR in reporter cells, similar to the known AhR activators 2,3,7,8-tetrachlorodibenzo-*p*-dioxin (TCDD) (Nebert et al., 1972) and *Mtb*-derived pigment Pht (Moura-Alves et al., 2014) (Figures 1A–1C, S1A, and S1B). Among the tested first-line TB drugs (group 1), we identified RFB as potent activator of the AhR (Figures 1A and S1C). Stimulation with RFB, or its major metabolite 25-O-deacetylrifabutin (25-O-DRFB), resulted in dose-dependent AhR activation (Figure S1C). Among newly approved drugs for the treatment of drug-resistant TB (groups 2–5), we identified bedaquiline (BDQ) and linezolid (LZD) as activators of the AhR (Figures S1D and S1E). Exposure to the specific synthetic AhR inhibitor CH-223191 (Kim et al., 2006) blocked the induction of luciferase activity upon stimulation with TCDD, Pht (Figures S1F and S1G), RFB, BDQ, and LZD (Figures S1H–S1J). Consistently, AhR knockdown showed a similar phenotype (Figures S1K–S1M). Several TB drugs did not activate the AhR but significantly decreased Pht-induced AhR activation when administered prior to stimulation with Pht (Figures 1B, 1C, and S1N–S1S). Pre-incubation with the first-line TB drugs rifampicin (RIF) and rifapentine (RPT) markedly decreased Pht-induced AhR activation (Figures 1B, 1C, and S1N). Similarly, stimulation with TB drugs of groups 3–5—including enrofloxacin (ERF), moxifloxacin (MXF), ethionamide (ETA), clofazimine (CFZ), and thiacetazone (THZ)—also decreased Pht-induced AhR activation (Figures S1O–S1S). Taken together, using THP-1 AhR reporter, we identified several first- and second-line TB drugs as potent modulators of the canonical AhR pathway (Table 1).

Both RFB and RIF are key first-line TB drugs (World Health Organization, 2016). Based on the observed opposing effects on AhR modulation, we further focused on the characterization of RFB- and RIF-mediated effects on the AhR as examples of TB drugs with AhR modulatory capacities. To exclude that AhR modulation mediated by RFB and RIF was because of impaired cell viability, we monitored lactate dehydrogenase release (LDH) and caspase-3/7 activity of reporter macrophages. No significant differences were observed under the conditions tested (Figures S2A and S2B). Similar to Pht, RFB induced the expression of AhR-dependent genes (*CYP1A1*, *CYP1B1*, and *AHRR*) in THP-1 macrophages, whereas *AHR* expression itself remained unaltered (Figures 1D and S2C). Consistently, in a murine hepatocyte cell line (Hepa-1c1c7), RFB activated the AhR in a dose-dependent manner (Figure S2D). Recently, it was reported that AhR activity can be modulated indirectly via dysregulation of CYP1A1 (Wincent et al., 2012). To evaluate whether inhibition of CYP1A1 by RFB activates the AhR indirectly, we measured CYP1A1 enzymatic activity. Stimulation of Hepa-1c1c7 cells with RFB led to a dose-dependent increase in enzymatic CYP1A1 activity, similar to stimulation with Pht or TCDD (Figures 1E and 1F). Thus, we exclude indirect AhR activation by CYP1A1 inhibition. In contrast, RIF stimulation of Hepa-1c1c7 cells did not induce CYP1A1 activity but profoundly inhibited Pht-induced CYP1A1 activity (Figures 1G and 1H). Our data suggest that both RFB and RIF are modulators of the canonical AhR pathway with opposing effects on AhR signaling.

RFB and RIF Bind to the AhR

To evaluate binding of TB drugs to the AhR, we tested ligand binding to a purified AhR protein by microscale thermophoresis (MST). MST allows measurement of protein-ligand interactions based on temperature-induced changes in the fluorescence of a target of interest (here, AhR) and a non-fluorescent ligand (Seidel et al., 2013). We confirmed binding of RIF (K_d 11.3 μM), RFB (K_d 16.1 μM), and the RFB metabolite 25-O-DRFB (approximately K_d 24.5 μM) to the AhR (Figures 2A–2C, S3A, and S3B). Importantly, binding to the AhR nuclear translocator (Arnt) was not observed, indicating the specificity of ligand binding to the AhR under the conditions tested. As a control, we tested binding of isoniazid (INH), another first-line TB drug, in which we observed no AhR modulation in the reporter assay (Table 1). Consistently, we did not detect binding of INH to the AhR (Figures S3A and S3C). We conclude that the first-line TB drugs RIF and RFB, as well as its metabolite 25-O-DRFB, bind to and modulate AhR activity, rendering anti-mycobacterial drugs a class of AhR ligands.

The atomic structure of the AhR ligand binding domain remains unknown. Therefore, despite being only predictive, computational-based molecular modeling studies are widely used to predict how different ligands bind to and modulate AhR functions (Pohjanvirta, 2011; Moura-Alves et al., 2014; Corrada et al., 2017; Mahiout et al., 2018). We applied molecular modeling and *in silico* docking to determine how RFB and RIF fit into the proposed binding pocket of the AhR (Moura-Alves et al., 2014). Despite structural similarities of the cyclic part between RFB and RIF, parts of their backbone conformations, orientations,

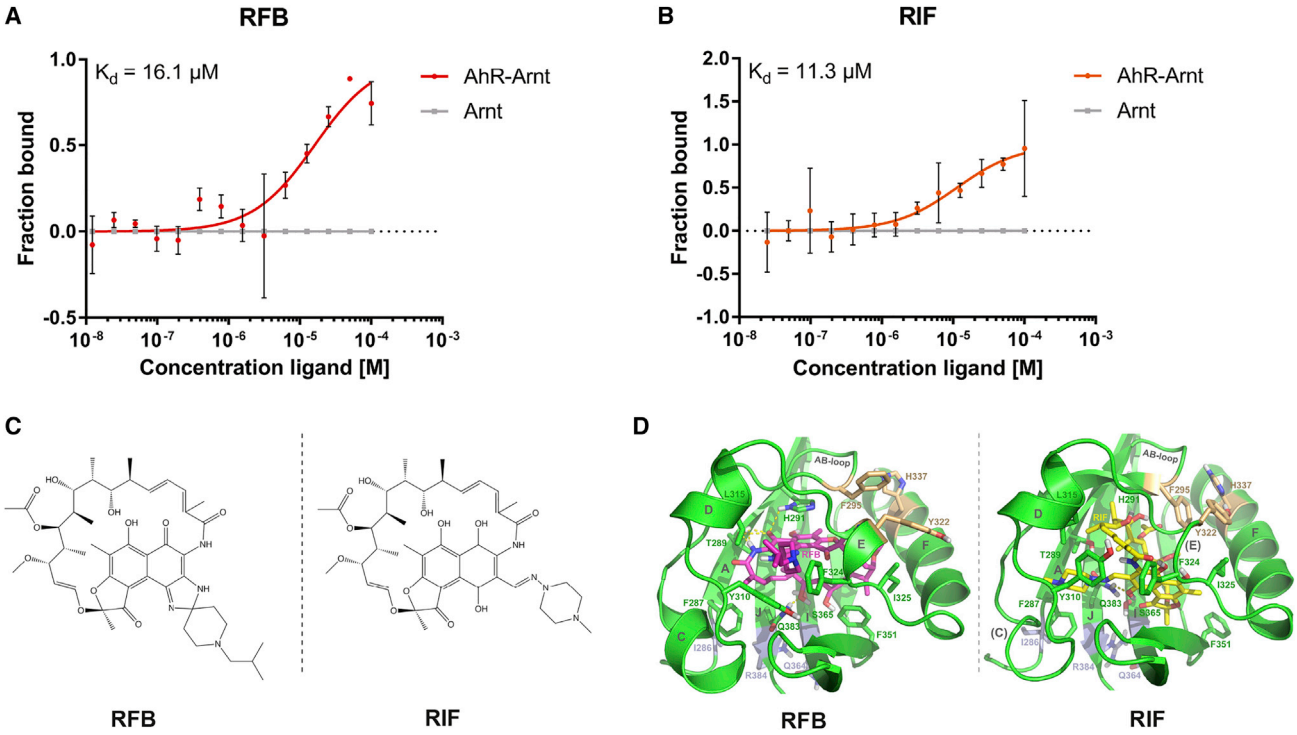

Figure 2. AhR Binding of TB Drugs

(A and B) AhR-binding studies of (A) RFB and (B) RIF to the AhR protein complex (AhR-Arnt) or Arnt alone using MST. Median ± SD of triplicates shown.

(C) Chemical structures of RFB and RIF.

(D) Best scoring ligand docking poses for RFB (left, magenta) and RIF (right, yellow) in the *in silico* model of the hAhR-PasB. H-bonds are depicted as yellow dotted lines; different conformations of the outward-oriented residues F295, Y322, and H337 are depicted in pale wheat; outward-oriented residues on the backside of the β sheet A, I, J (Ile286, Gln364, and Arg384) that are able to interact with PasA of Arnt are depicted in pale blue.

See also Figure S3 and Table S1.

and size of the substituents differ (Figure 2C). While RFB and RIF do not resemble prototypic AhR ligands (Figures 2C and S3D), molecular modeling and *in silico* docking resulted in putative fitting into the ligand binding pocket of the AhR-PasB model, with only few possible configurations (calculated ΔG binding: RFB = −130.16 kcal/mol and RIF = −125.21 kcal/mol and −118.66 kcal/mol) (Table S1). Interestingly, docking of RFB and RIF into the AhR binding pocket resulted in different orientations, suggesting dissimilar interaction profiles (Figure 2D; Table S1). Within the AhR-PasB ligand binding pocket, RFB formed multiple hydrogen bonds with the side chains of Thr289, His291, Ser365, and Gln383, altering the existing H-bond network between these residues. Such rearrangements influence the structural adjustment, especially the N- and C-terminal endings of particular β strands (segments A, I, and J) of the β sheet and the AB-loop, which leads to a constrained backbone conformation at two locations: (1) at the AB-loop as part of the interface between the AhR and the PasB of Arnt (Corrada et al., 2017;'Corrada et al., 2016), comprised of Phe295 (AB-loop), Tyr322 (helix E), and His337 (helix F) (Figures 2D, S3E, and S3F); and (2) at the interface between the AhR and the PasA of Arnt (Figure S3E) that is formed by outward-oriented residues on the N-terminal end of β strand A (Ile286) and/or on the backside of β strands I and J (Gln364 and Arg384) (Figure 2D). Compared with RFB, both RIF and the specific AhR inhibitor CH-223191 (Figures 2D, S3D, and S3F; Table S1) formed considerably less H-bonds to residues on the β strands A, I, and J. Such differences in RFB, RIF, and CH-223191 binding to the AhR lead to opposing conformational influences on the two interaction positions, potentially impacting AhR activation.

Modulation of the AhR Impairs Macrophage Phagocytosis

We further evaluated potential effects of ligand-induced AhR modulation in the context of infection and TB drug therapy. We assessed whether the AhR could play a role in macrophage phagocytosis of *Mtb*. Inhibition of the AhR by CH-223191 in THP-1 macrophages reduced the uptake of *Mtb* H37Rv (Figure 3A). Likewise, AhR-inhibition decreased uptake of fluorescently labeled *Mtb* H37Rv, paralleled by a reduction in the proportion of *Mtb*-harboring cells (Figures 3B, 3C, and S4A). Exposure to CH-223191 did not affect *Mtb* or macrophage viability (Figures S4B–S4F). Consistently, knockdown of the AhR in THP-1 macrophages likewise resulted in reduced uptake of *Mtb* H37Rv (Figure 3D). To further characterize the role of the AhR in phagocytosis, we used the fungal glucan zymosan conjugated to a pH-sensitive dye (pHrodo), which allows visualization of phagosomal uptake and acidification (Queval et al., 2017). Consistent with *Mtb* phagocytosis, the proportion of zymosan-containing macrophages and the rate of internalization were

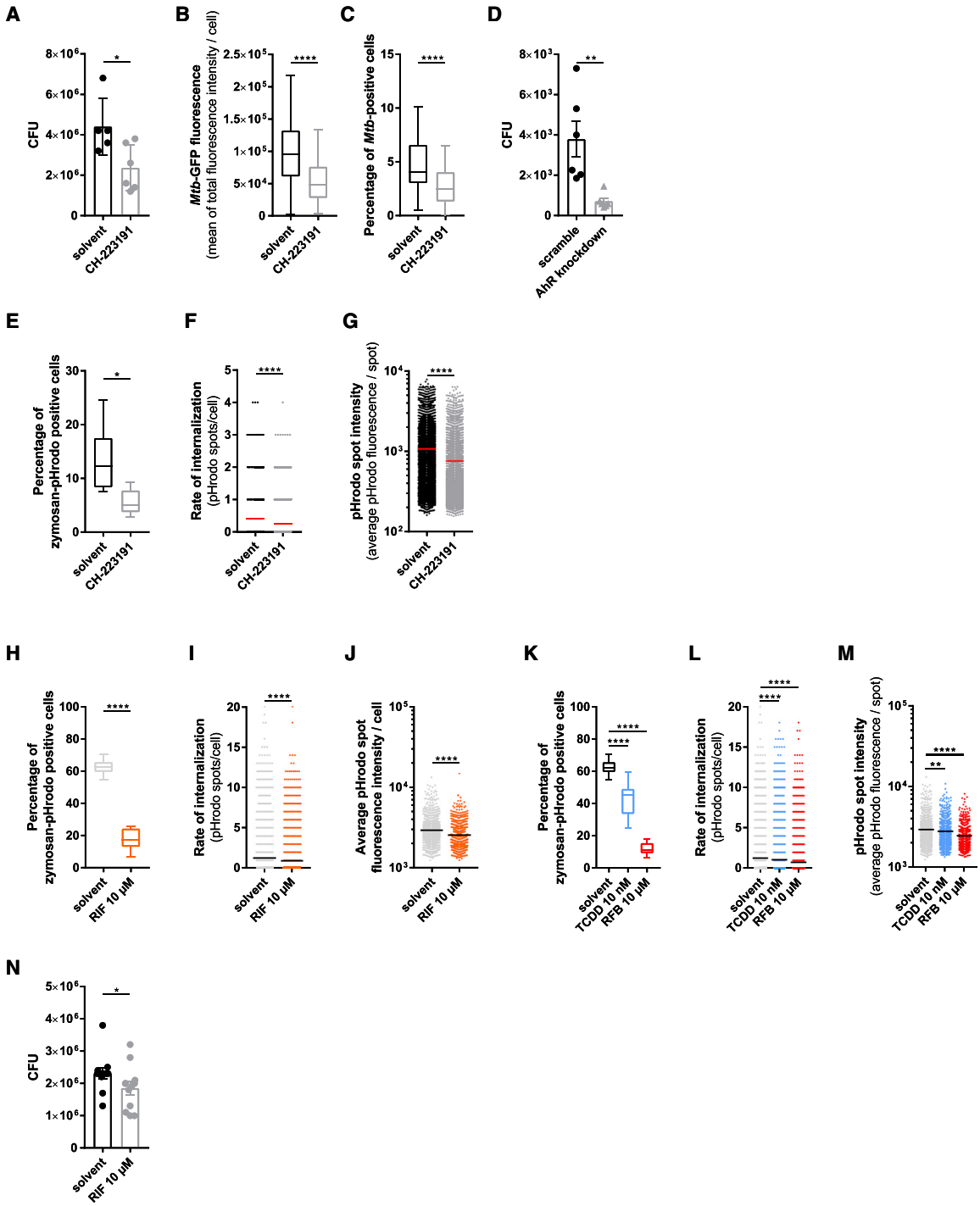

Figure 3. Modulation of Phagocytosis by AhR

(A–D) Uptake of *Mtb* multiplicity of infection (MOI) of 10 by AhR proficient or deficient (12 μM CH-223191 pre-treatment for 2 h or shRNA knockdown) THP-1 macrophages after 4 h, measured by (A and D) CFU (*Mtb* H37Rv) or (B and C) microscopy (*Mtb*-GFP H37Rv).

(E–G) Phagocytosis of zymosan-pHrodo by macrophages (RAW264.7) 2 h after pre-incubation with 12 μM CH-223191 or dimethyl sulfoxide (DMSO; solvent) for 2 h. (E) Percentage of zymosan-pHrodo positive cells, (F) rate of zymosan-pHrodo internalization, and (G) average intensity of internalized pHrodo.

(H–M) Phagocytosis of zymosan-pHrodo by macrophages (THP-1) 2 h after pre-incubation with (H–J) RIF and (K–M) TCDD or RFB for 2 h. (H and K) Percentage of zymosan-pHrodo positive cells, (I and L) rate of internalization of zymosan-pHrodo, and (J and M) average intensity of internalized pHrodo.

(N) Uptake of RIF-resistant *Mtb* MOI of 10 by THP-1 macrophages pre-treated for 2 h with 10 μM RIF or DMSO (solvent) after 4 h, measured by CFU.

(A and D) 1 representative of n = 2 independent experiments.

(B, C, and E–M) 1 representative of n = 3 independent experiments.

(legend continued on next page)

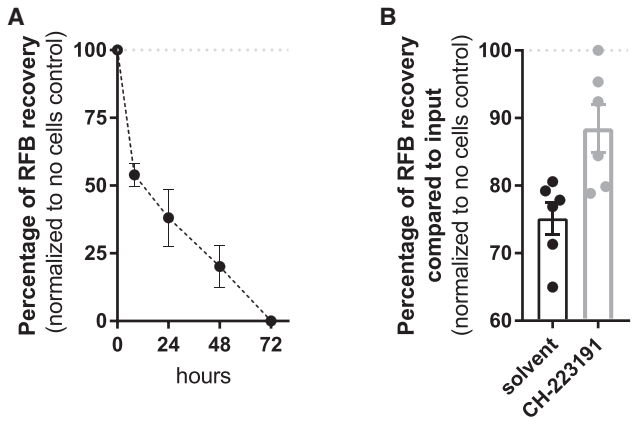

Figure 4. AhR Inhibition in Human Hepatocytes Affects RFB Availability

(A) Percentage of RFB recovery from HepaRG culture supernatants over time compared with no cells control for each time point. 1 representative of n = 3 independent experiments. Mean ± SD shown.

(B) Percentage of RFB recovery from HepaRG culture supernatants in the presence or absence of CH-223191 after 48 h compared with the input and normalized to no cells control. Pooled data from n = 2 independent experiments. Mean ± SEM shown.

See also Figure S5.

decreased upon AhR inhibition (Figures 3E and 3F). AhR inhibition also reduced the pHrodo fluorescence intensity of internalized zymosan, indicating an AhR-dependent impact on macrophage phagosomal acidification (Figure 3G). Our data suggest a role for the AhR in macrophage phagocytosis of *Mtb* and the fungal glucan zymosan.

We extended our investigation of AhR-dependent phagocytosis to other AhR ligands, including TB drugs. The AhR antagonist RIF potently inhibited uptake of zymosan-pHrodo by macrophages, indicated by reduced numbers of zymosan-containing cells and the rate of internalization (Figures 3H and 3I). Moreover, RIF impaired phagosomal acidification, similar to the synthetic AhR inhibitor (Figures 3G and 3J). Notably, a similar phenotype was observed upon exposure to the AhR agonists TCDD and RFB (Figures 3K–3M). In contrast, INH, which neither binds nor modulates AhR, did not impair phagocytosis (Figures S4G–S4I). To further explore RIF-elicited effects on the AhR in the absence of a direct antimicrobial effect on *Mtb*, we took advantage of a RIF-resistant *Mtb* strain. Similar to what we observed for zymosan-pHrodo, RIF treatment of macrophages reduced uptake of the RIF-resistant patient isolate (Figure 3N). RIF resistance was confirmed by monitoring cultural growth in the presence or absence of RIF in comparison with a drug-sensitive *Mtb* patient isolate (Figures S4J and S4K), and by next generation sequencing and drug-susceptibility testing (Table S2). We conclude that ligand-induced AhR modulation impairs macrophage phagocytosis. Moreover, we identified a yet-unknown host-directed effect of the TB drugs RIF and RFB on macrophage phagocytosis.

AhR Is Involved in Metabolism of RFB

Pharmacokinetic and pharmacodynamic factors markedly influence drug availability and efficacy, which are essential for successful treatment (Rowland and Tozer, 2011). The AhR is a central regulator of xenobiotic metabolism (Stockinger et al., 2014). Hence, we evaluated whether the AhR is involved in the metabolism of RFB. We made use of the human hepatic stem cell line HepaRG, which has AhR expression levels reported to be comparable with primary human hepatocytes (Guillouzo et al., 2007). Moreover, HepaRG cells express multiple functional phase 1 and 2 drug metabolizing enzymes, rendering them suitable for studies on xenobiotic metabolism (Guillouzo et al., 2007). We monitored RFB clearance from cell culture supernatants using ultra-performance liquid chromatography (UPLC). We observed continuous elimination of RFB from HepaRG cell cultures (Figure 4A). Strikingly, RFB recovery from supernatants of AhR-inhibited cells was higher when compared with solvent controls (Figure 4B). Importantly, treatment of HepaRG cells with CH-223191 and/or RFB did not impair cell viability at the concentrations used (Figures S5A and S5B). Our data suggest that the AhR is involved in hepatic metabolism of RFB and that inhibiting the AhR reduces RFB metabolism, ultimately affecting its availability.

In Vivo Modulation of AhR by TB Drugs

The zebrafish (*Danio rerio*) has emerged as valuable animal model to study toxicology (Roper and Tanguay, 2018) and the mechanisms of disease, including TB (Van Leeuwen et al., 2015). Increasingly, zebrafish have been harnessed for high-throughput *in vivo* screenings of novel drug candidates, such as antimicrobials (Zhong and Lin, 2011; Dalton et al., 2017). We used zebrafish to validate our *in vitro* findings. Similar to what we observed in cell lines, exposure of zebrafish embryos to RFB induced AhR downstream target genes, such as *ahrra* (Evans et al., 2005), *ahrrb* (Evans et al., 2005), and *cyp1a* (Prasch et al., 2003), in an AhR-dependent manner (Figure 5A). Furthermore, *in vivo* EROD assays detected increased Cyp1a enzymatic activity upon RFB exposure, similar to that induced by Pht (Figure 5B). CH-223191 blocked *cyp1a* gene expression (Figure 5A) and induction of Cyp1a enzymatic activity (Figure 5C). Exposure of zebrafish embryos to increasing concentrations of RIF did not induce Cyp1a activity (Figure 5D); instead, RIF potently inhibited TCDD-induced Cyp1a enzymatic activity (Figure 5E). We did not detect toxicity in zebrafish for any of the ligands and conditions tested (Figures S6A and S6B). To evaluate whether the AhR also plays a role in RFB metabolism *in vivo*, we exposed zebrafish embryos to RFB in the water and collected samples at 4 days post-exposure. In

(N) Pooled data from n = 2 independent experiments.

Shown as (A and D) mean ± S.D., (B, C, E, H, and K) boxplot with Tukey whiskers, (F, G, I, J, L, and M) scatter dot plot with mean, (N) mean ± SEM.

(A–M) Unpaired t test. *p ≤ 0.05, **p ≤ 0.01, ****p ≤ 0.0001.

(N) Mann-Whitney test. *p ≤ 0.05.

See also Figure S4 and Table S2.

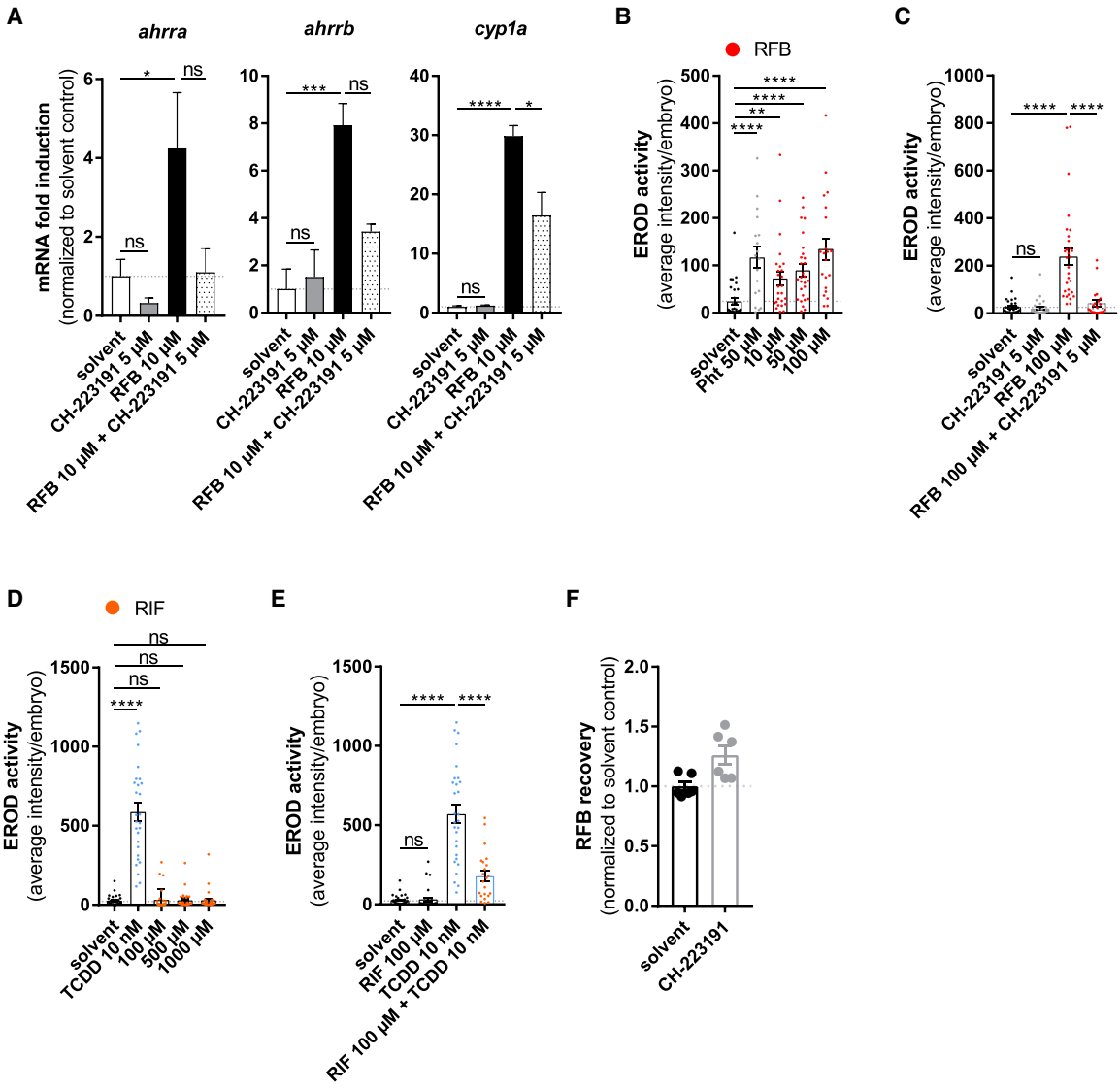

Figure 5. AhR Modulation by RFB and RIF *In Vivo*

(A) Gene-expression analysis of AhR-target genes in 2 days post-fertilization (dpf) zebrafish embryos upon 4 h of stimulation with RFB, in the presence or absence of CH-223191. Triplicates, each consisting of 12 zebrafish embryos pooled. Mean ± SD shown.

(B–E) *Cyp1a* enzymatic activity (EROD) in 2 dpf embryos treated for 4h with (B) Pht or increasing concentrations of RFB, (C) with RFB in the presence or absence of CH-223191, (D) with TCDD or increasing concentrations of RIF, and (E) with TCDD in the presence or absence of RIF. Each data point depicts an individual zebrafish embryo. Mean ± SEM shown.

(F) Recovery of RFB from the water of zebrafish embryos after 4 days of exposure to 5 µM RFB in the presence of 10 µM CH-223191 compared with DMSO (solvent) control.

(A–E) 1 representative of n = 3 independent experiments.

(F) Pooled data from n = 2 independent experiments. Mean ± SEM shown.

(A-F) Unpaired t test. ns (not significant), *p ≤ 0.05, **p ≤ 0.01, ***p ≤ 0.01 ****p ≤ 0.0001.

See also Figure S6.

agreement with results from human hepatocyte cultures (Figure 4B), AhR inhibition in zebrafish resulted in higher RFB recovery compared with controls (Figure 5F). Altogether, we demonstrate that *in vivo* exposure of zebrafish embryos to TB drugs, such as RFB and RIF, modulate AhR downstream responses including the regulation of gene expression and drug metabolism.

Modulation of AhR during Mycobacterial Infection and Treatment *In Vivo*

We interrogated whether AhR-dependent RFB degradation affects the efficacy of drug treatment *in vivo*. To this end, we made use of the zebrafish-*Mycobacterium marinum* infection model of mycobacterial pathogenesis (Van Leeuwen et al., 2015). Stimulation of AhR reporter macrophages with filtered

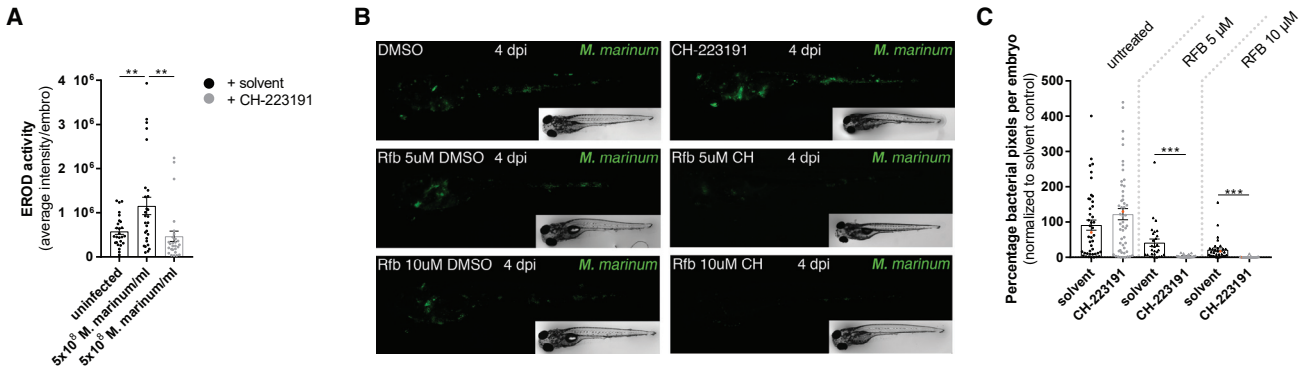

Figure 6. AhR Modulation during *M. marinum* Infection and RFB Treatment *In Vivo*

(A) Cyp1a enzymatic activity (EROD) in 2 dpf embryos exposed to *M. marinum* for 24 h in E3 medium, in the presence or absence of 10 μM CH-223191. 1 representative of n = 3 independent experiments. Mean ± SD shown.

(B and C) Bacterial loads in zebrafish embryos at 4 d post-systemic infection with Wasabi-expressing *M. marinum* (200 CFU), untreated or treated with RFB for 3 d, in the presence or absence of 10 μM CH-223191. 1 representative of n = 2 independent experiments. Mean ± SEM shown.

(B) Representative micrographs.

(C) Quantification of Wasabi-expressing *M. marinum* pixels per whole embryo.

(A and C) Each data point depicts an individual zebrafish embryo, (C) while orange symbols indicate the individuals that were chosen as representative micrograph. Unpaired t test. *p ≤ 0.05, **p ≤ 0.01, ****p ≤ 0.0001.

See also Figures S7 and S8.

M. marinum culture supernatants induced AhR activation (Figure S7A), similar to *Mtb* and *Mycobacterium bovis* Bacillus Calmette-Guérin (BCG; Moura-Alves et al., 2014). Exposure of zebrafish embryos to *M. marinum* by immersion, a natural route of infection (Dalton et al., 2017), induced Cyp1a enzymatic activity in zebrafish embryos, as did TCDD (Figures 6A and S7B). Cyp1a enzymatic activation was abrogated by CH-223191 (Figure 6A). Our data support previous findings that mycobacterial infection activates AhR signaling in other models, including mouse (Moura-Alves et al., 2014). Hence, zebrafish represent a suitable *in vivo* model to study the role of the AhR during infection and drug treatment.

Intravenous infection of zebrafish embryos with *M. marinum* followed by AhR inhibition (CH-223191) resulted in higher bacterial burden in embryos when compared with controls (Figures 6B and 6C). This is in line with the increased bacterial burden observed in AhR knockout mice infected with *Mtb* (Moura-Alves et al., 2014). Importantly, we did not identify any direct effect of the specific AhR-inhibitor CH-223191 on bacterial growth or fluorescence (Figures S8A–S8C), nor did we observe adjuvant effects of CH-223191 during RFB treatment (Figures S8D and S8E). Interestingly and in agreement with our *in vitro* results, we observed a delay in macrophage phagocytosis of *M. marinum* upon CH-233191 treatment in zebrafish embryos *in vivo* (Figures S8F and S8G). Based on our results that suggest a role for the AhR in RFB metabolism, we evaluated whether inhibition of the AhR in *M. marinum*-infected zebrafish embryos affects efficacy of RFB treatment. Treatment with RFB dose dependently decreased bacterial loads (Figures 6B and 6C), confirming antimicrobial activity of RFB in *M. marinum*-infected zebrafish embryos. Remarkably, AhR inhibition by CH-223191 enhanced RFB-mediated bacterial killing compared with AhR-proficient controls (Figures 6B and 6C), correlating with higher drug concentrations upon AhR inhibition (Figures 4B and 5F). Of note, we did not observe AhR-dependent differences in bacterial killing upon RIF treatment in zebrafish embryos as well as changes in RIF metabolism upon AhR inhibition (Figures S8H and S8I). Taken together, our data unveil that the AhR concomitantly senses infection and drug treatment, thereby playing a central role in host-pathogen interactions and treatment in TB.

DISCUSSION

Here, we demonstrate that differential modulation of the AhR by TB drugs influences both host defense and treatment outcome. Hence, the AhR is a critical denominator in TB. More precisely, we demonstrate that: (1) TB drugs, including the first-line drugs RFB and RIF, are AhR ligands; (2) AhR modulation by both RFB and RIF impairs macrophage phagocytosis and phagosomal acidification; (3) RFB and RIF differentially regulate AhR target gene expression and enzymatic Cyp1a activity *in vitro* and in zebrafish; (4) inhibition of the AhR impairs metabolism of RFB in human hepatocytes and in zebrafish; and (5) pharmacological inhibition of the AhR augments RFB-mediated antimicrobial activity in *M. marinum*-infected zebrafish embryos.

After aerogenic infection, macrophages are among the first host cells to encounter *Mtb* (Gengenbacher and Kaufmann, 2012). We demonstrate that inhibition of the AhR affects phagocytosis of both *Mtb* and zymosan by a currently unknown mechanism. Previous studies showed an involvement of the AhR in actin polymerization and cytoskeleton remodeling (Carvajal-Gonzalez et al., 2009; Angeles-Floriano et al., 2016). Thus, it is tempting to speculate that AhR-mediated regulation of this process can potentially impact phagocytosis, although further studies are needed to evaluate this hypothesis. Our findings are reminiscent of a recent study reporting that AhR activation by the opportunistic pathogenic yeast *Candida albicans* promotes endocytosis by epithelial cells and that AhR inhibition reduces fungal invasion (Solis et al., 2017). Consistently, exposure to the AhR ligands RFB and RIF likewise reduced macrophage

phagocytosis. Our observations are in agreement with earlier studies reporting the effects of antibiotics on macrophage phagocytosis (Nishida et al., 1976; Bode et al., 2014). We conclude that impaired phagocytosis by TB drugs impacts host defense and thereby influences therapy outcome. Because of the vast spectrum of modulatory AhR ligands, this mechanism should be taken into consideration for: (1) antibiotic treatment of bacterial infections, in which phagocytosis plays a critical role, such as TB; and (2) drug treatment in the presence of environmental AhR modulators, which could affect host defense and drug availability. Environmental risk factors for AhR modulation may set a basal threshold, which affects diverse pathophysiological pathways. For example, cigarette smoke contains several potent AhR agonists, including TCDD (Muto and Takizawa, 1989) and benzo(a)pyrene (Stedman, 1968). The AhR has been shown to regulate cigarette-smoke-induced cyclooxygenase-2 (COX-2) and prostaglandin E_2 (PGE_2) (Martey et al., 2005) expression, the latter being critical in immunopathogenesis of TB (Rangel Moreno et al., 2002). It is therefore tempting to envision that AhR signaling could participate in the heightened risk of TB for smokers (Alcaide et al., 1996) and in their poor therapy outcome (Leung et al., 2015; Yen et al., 2014).

The currently recommended treatment regimen of patients with drug-susceptible TB consists of at least four drugs given over an extended period of time (2-month intensive treatment with INH, RIF, PZA, and EMB, followed by 4-month continuation treatment with INH and RIF) (World Health Organization, 2017). We identified TB drugs that modulate the AhR pathway in opposite ways including RFB and RIF, which activated or inhibited AhR, respectively. In combination therapy, this could result in synergistic or antagonistic effects and thus should be taken into consideration when formulating novel multidrug treatment regimens for TB. The emergence of MDR- and XDR-TB has become a global public health threat (World Health Organization, 2019). Treatment duration (Olofsson and Cars, 2007) and suboptimal drug concentrations (DeRyke et al., 2006; Mitchison, 1998) promote the development of AMR. Drug metabolism influences duration and intensity of pharmacological action and is therefore considered critical for AMR selection (Baquero et al., 1997; Negri et al., 2000). Here, targeting the AhR by a specific small-molecule inhibitor reduced the metabolism of RFB, resulting in elevated drug concentrations and increased RFB-mediated antimicrobial activity. We conclude that modulation of the AhR affects overall drug availability and, potentially, the development of AMR. Identification of suitable HDT targets is of vital importance to counteract the rising threat posed by AMR in TB. Given the central role of the AhR in infection and treatment, we propose the AhR as a candidate target for adjunct HDT in TB. Of note, targeting the AhR has already been harnessed in other disease models (Yeste et al., 2012, 2016; Zelante et al., 2013; Parks et al., 2014; Cervantes-Barragan et al., 2017; Smith et al., 2017; Lozza et al., 2019). However, because of its vast ligand binding capacity (e.g., allowing sensing of both bacteria and drug treatment) and its implication in multiple cellular and tissue mechanisms, targeting the AhR might carry potential risks that need to be further evaluated. The work presented here serves as the foundation for future studies to ultimately verify the suitability of the AhR as HDT in TB, looking at both potential benefits and risks of such therapeutic intervention.

STAR★METHODS

Detailed methods are provided in the online version of this paper and include the following:

- KEY RESOURCES TABLE
- LEAD CONTACT AND MATERIALS AVAILABILITY
- EXPERIMENTAL MODEL AND SUBJECT DETAILS
  - Bacterial Strains and Maintenance
  - Cell Culture and Maintenance
  - Zebrafish Model
- METHOD DETAILS
  - Gene Expression Analysis by qRT-PCR
  - Luciferase Reporter Assay
  - siRNA Knockdown of AhR
  - EROD Activity *In Vitro*
  - LDH Release Assay
  - Caspase-3/7 Activity Assay
  - *In Vitro* Infections and Analysis
  - Broth Dilution Assay
  - Zymosan-pHrodo Phagocytosis Assays
  - Rifabutin Metabolism
  - Molecular Modeling
  - AhR Binding Studies Using MST
  - Zebrafish Chemical Stimulations
  - Zebrafish Cyp1a Enzymatic Activity
  - Zebrafish Toxicity
  - Zebrafish Infection
  - RFB Treatment of *M. marinum*-Infected Zebrafish
- QUANTIFICATION AND STATISTICAL ANALYSIS
- DATA AND CODE AVAILABILITY

SUPPLEMENTAL INFORMATION

Supplemental Information can be found online at https://doi.org/10.1016/j.chom.2019.12.005.

ACKNOWLEDGMENTS

The authors acknowledge those who have provided tools and materials for this study. Expression plasmid pET30-EK/LIC-Arnt was a gift from Oliver Daumke and Kathrin Schulte (Max Delbruck Center, Berlin, Germany). Stefan Niemann, Katharina Kranzer, and Anne Witt (Forschungszentrum Borstel, Borstel, Germany) kindly provided and characterized *Mtb* patient isolates. Christiane Guguen-Guillouzo, Philippe Gripon, and Christian Trepo kindly made the HepaRG cell line available. Clemens Grabher (Karlsruhe Institute of Technology, Karlsruhe, Germany) and Daniela Panakova (Max Delbruck Center, Berlin, Germany) provided the zebrafish AB WT strain. We acknowledge Norman Fielko, Jens Otto, Andrey Fadeev (Max Planck Institute for Infection Biology, Berlin, Germany), and Mariana Simões (Max Delbruck Center, Berlin, Germany) for zebrafish breedings. The Graphical Abstract was created with BioRender.com. This work was generously supported by the SPP 1937 DFG Project KA 573/6-1 (SPP 1937) and an internal grant of the Max Planck Society to S.H.E.K. as well as by the International Max Planck Research School for Infectious Diseases and Immunology (IMPRS-IDI) to A.P. and A.S.

AUTHOR CONTRIBUTIONS

Conceptualization, A.P., S.H.E.K., and P.M.-A.; Methodology, A.P., A.S., S.H.E.K., M.v.d.V., M.S., A.H.M., A.K., G.K., J.P., and P.M.-A.; Formal Analysis, A.P., S.H.E.K., M.v.d.V., A.K., G.K., J.P., and P.M.-A.; Investigation, A.P., A.S., G.P., G.K., U.G.-B., M.K., M.v.d.V., R.H., A.K., G.K., J.P., and P.M.-A.; Funding Acquisition, A.P., A.S., and S.H.E.K.; Writing – Original Draft, A.P., S.H.E.K., and

P.M.-A.; Writing – Review & Editing, A.P., S.H.E.K., and P.M.-A.; Visualization, A.P. and P.M.-A.; Supervision, A.H.M., G.K., S.H.E.K., and P.M.-A.

DECLARATION OF INTERESTS

The authors declare no competing interests.

Received: April 8, 2019
Revised: October 30, 2019
Accepted: December 6, 2019
Published: December 31, 2019

REFERENCES

Alcaide, J., Altet, M.N., Plans, P., Parrón, I., Folguera, L., Saltó, E., Domínguez, A., Pardell, H., and Salleras, L. (1996). Cigarette smoking as a risk factor for tuberculosis in young adults: a case-control study. Tuber Lung Dis. *77*, 112–116.

Angeles-Floriano, T., Roa-Espitia, A.L., Baltiérrez-Hoyos, R., Cordero-Martínez, J., Elizondo, G., and Hernández-González, E.O. (2016). Absence of aryl hydrocarbon receptor alters CDC42 expression and prevents actin polymerization during capacitation. Mol. Reprod. Dev. *83*, 1015–1026.

Baquero, F., Negri, M.C., Morosini, M.I., and Blázquez, J. (1997). The antibiotic selective process: concentration-specific amplification of low-level resistant populations. Ciba Found Symp. *207*, 93–105.

Benard, E.L., van der Sar, A.M., Ellett, F., Lieschke, G.J., Spaink, H.P., and Meijer, A.H. (2012). Infection of zebrafish embryos with intracellular bacterial pathogens. J Vis Exp. 3781, https://doi.org/10.3791/3781.

Bode, C., Diedrich, B., Muenster, S., Hentschel, V., Weisheit, C., Rommelsheim, K., Hoeft, A., Meyer, R., Boehm, O., Knuefermann, P., and Baumgarten, G. (2014). Antibiotics regulate the immune response in both presence and absence of lipopolysaccharide through modulation of Toll-like receptors, cytokine production and phagocytosis in vitro. Int. Immunopharmacol. *18*, 27–34.

Carvajal-Gonzalez, J.M., Mulero-Navarro, S., Roman, A.C., Sauzeau, V., Merino, J.M., Bustelo, X.R., and Fernandez-Salguero, P.M. (2009). The dioxin receptor regulates the constitutive expression of the vav3 proto-oncogene and modulates cell shape and adhesion. Mol. Biol. Cell *20*, 1715–1727.

Cervantes-Barragan, L., Chai, J.N., Tianero, M.D., Di Luccia, B., Ahern, P.P., Merriman, J., Cortez, V.S., Caparon, M.G., Donia, M.S., Gilfillan, S., et al. (2017). *Lactobacillus reuteri* induces gut intraepithelial $CD4^+CD8\alpha\alpha^+$ T cells. Science *357*, 806–810.

Corrada, D., Soshilov, A.A., Denison, M.S., and Bonati, L. (2016). Deciphering Dimerization Modes of PAS Domains: Computational and Experimental Analyses of the AhR:ARNT Complex Reveal New Insights Into the Mechanisms of AhR Transformation. PLoS Comput Biol. *12*, e1004981. Published online June 13, 2016. https://doi.org/10.1371/journal.pcbi.1004981.

Corrada, D., Denison, M.S., and Bonati, L. (2017). Structural modeling of the AhR:ARNT complex in the bHLH-PASA-PASB region elucidates the key determinants of dimerization. Mol. Biosyst. *13*, 981–990.

Dalton, J.P., Uy, B., Okuda, K.S., Hall, C.J., Denny, W.A., Crosier, P.S., Swift, S., and Wiles, S. (2017). Screening of anti-mycobacterial compounds in a naturally infected zebrafish larvae model. J Antimicrob Chemother. *72*, 421–427.

DeRyke, C.A., Lee, S.Y., Kuti, J.L., and Nicolau, D.P. (2006). Optimising dosing strategies of antibacterials utilising pharmacodynamic principles: impact on the development of resistance. Drugs *66*, 1–14.

Evans, B.R., Karchner, S.I., Franks, D.G., and Hahn, M.E. (2005). Duplicate aryl hydrocarbon receptor repressor genes (ahrr1 and ahrr2) in the zebrafish Danio rerio: structure, function, evolution, and AHR-dependent regulation in vivo. Arch. Biochem. Biophys. *441*, 151–167.

Gengenbacher, M., and Kaufmann, S.H.E. (2012). Mycobacterium tuberculosis: success through dormancy. FEMS Microbiol Rev. *36*, 514–532.

Guillouzo, A., Corlu, A., Aninat, C., Glaise, D., Morel, F., and Guguen-Guillouzo, C. (2007). The human hepatoma HepaRG cells: A highly differentiated model for studies of liver metabolism and toxicity of xenobiotics. Chem Biol Interact. *168*, 66–73.

Gutiérrez-Vázquez, C., and Quintana, F.J. (2018). Regulation of the Immune Response by the Aryl Hydrocarbon Receptor. Immunity *48*, 19–33.

Huang, N., Chelliah, Y., Shan, Y., Taylor, C.A., Yoo, S.-H., Partch, C., Green, C.B., Zhang, H., and Takahashi, J.S. (2012). Crystal structure of the heterodimeric CLOCK:BMAL1 transcriptional activator complex. Science *337*, 189–194.

Hubbard, T.D., Murray, I.A., and Perdew, G.H. (2015). Indole and Tryptophan Metabolism: Endogenous and Dietary Routes to Ah Receptor Activation. Drug Metab. Dispos. *43*, 1522–1535.

Kaufmann, S.H., Rubin, E., and Zumla, A. (2015). Tuberculosis (Cold Spring Harbor Laboratory Press).

Kaufmann, S.H.E., Dorhoi, A., Hotchkiss, R.S., and Bartenschlager, R. (2018). Host-directed therapies for bacterial and viral infections. Nat. Rev. Drug Discov. *17*, 35–56.

Kawajiri, K., and Fujii-Kuriyama, Y. (2017). The aryl hydrocarbon receptor: a multifunctional chemical sensor for host defense and homeostatic maintenance. Exp. Anim. *66*, 75–89.

Kim, S.-H., Henry, E.C., Kim, D.-K., Kim, Y.-H., Shin, K.J., Han, M.S., Lee, T.G., Kang, J.-K., Gasiewicz, T.A., Ryu, S.H., and Suh, P.-G. (2006). Novel compound 2-methyl-2H-pyrazole-3-carboxylic acid (2-methyl-4-o-tolylazo-phenyl)-amide (CH-223191) prevents 2,3,7,8-TCDD-induced toxicity by antagonizing the aryl hydrocarbon receptor. Mol. Pharmacol. *69*, 1871–1878.

Kolloli, A., and Subbian, S. (2017). Host-Directed Therapeutic Strategies for Tuberculosis. Front. Med. (Lausanne) *4*, 171.

Leung, C.C., Yew, W.W., Chan, C.K., Chang, K.C., Law, W.S., Lee, S.N., Tai, L.B., Leung, E.C.C., Au, R.K.F., Huang, S.S., and Tam, C.M. (2015). Smoking adversely affects treatment response, outcome and relapse in tuberculosis. Eur. Respir. J. *45*, 738–745.

Liew, W.C., and Orbán, L. (2014). Zebrafish sex: a complicated affair. Brief. Funct. Genomics *13*, 172–187.

Lozza, L., Moura-Alves, P., Domaszewska, T., Lage Crespo, C., Streata, I., Kreuchwig, A., Puyskens, A., Bechtle, M., Klemm, M., Zedler, U., et al. (2019). The Henna pigment Lawsone activates the Aryl Hydrocarbon Receptor and impacts skin homeostasis. Sci. Rep. *9*, 10878.

Mahiout, S., Tagliabue, S.G., Nasri, A., Omoruyi, I.M., Pettersson, L., Bonati, L., and Pohjanvirta, R. (2018). In vitro toxicity and in silico docking analysis of two novel selective AH-receptor modulators. Toxicol In Vitro. *52*, 178–188.

Martey, C.A., Baglole, C.J., Gasiewicz, T.A., Sime, P.J., and Phipps, R.P. (2005). The aryl hydrocarbon receptor is a regulator of cigarette smoke induction of the cyclooxygenase and prostaglandin pathways in human lung fibroblasts. Am J Physiol Lung Cell Mol Physiol. *289*, L391–L399.

Mitchison, D.A. (1998). How drug resistance emerges as a result of poor compliance during short course chemotherapy for tuberculosis. Int J Tuber Lung Dis. *2*, 10–15.

Mohammadi-Bardbori, A., and Mohammadi-Bardbori, A. (2014). Assay for quantitative determination of CYP1A1 enzyme activity using 7-Ethoxyresorufin as standard substrate (EROD assay). Protoc. Exch.

Motta, S., Minici, C., Corrada, D., Bonati, L., and Pandini, A. (2018). Ligand-induced perturbation of the HIF-2α:ARNT dimer dynamics. PLoS Comput Biol. *14*, e1006021. Published online February 28, 2018. https://doi.org/10.1371/journal.pcbi.1006021.

Moura-Alves, P., Faé, K., Houthuys, E., Dorhoi, A., Kreuchwig, A., Furkert, J., Barison, N., Diehl, A., Munder, A., Constant, P., et al. (2014). AhR sensing of bacterial pigments regulates antibacterial defence. Nature *512*, 387–392.

Muto, H., and Takizawa, Y. (1989). Dioxins in cigarette smoke. Arch. Environ. Health *44*, 171–174.

Nacci, D., Coiro, L., Kuhn, A., Champlin, D., Munns, W., Specker, J., and Cooper, K. (1998). Nondestructive indicator of ethoxyresorufin- O -deethylase activity in embryonic fish. Environmental Toxicology and Chemistry. *17*, 2481–2486.

Nebert, D.W., Goujon, F.M., and Gielen, J.E. (1972). Aryl hydrocarbon hydroxylase induction by polycyclic hydrocarbons: simple autosomal dominant trait in the mouse. Nat. New Biol. *236*, 107–110.

Negri, M.C., Lipsitch, M., Blázquez, J., Levin, B.R., and Baquero, F. (2000). Concentration-dependent selection of small phenotypic differences in TEM beta-lactamase-mediated antibiotic resistance. Antimicrob. Agents Chemother. *44*, 2485–2491.

Nezhinsky, A.E., Stoop, E., van der Sar, A., and Verbeek, F.J. (2012). Numerical Analysis of Image based High Throughput Zebrafish Infection Screens-Matching Meaning with Data.. *Proceedings of the International Conference on Bioinformatics Models, Methods and Algorithms - Volume 1: BIOINFORMATICS* (BIOSTEC 2012), pp. 257–262.

Nishida, M., Mine, Y., Nonoyama, S., and Yokota, Y. (1976). Effect of antibiotics on the phagocytosis and killing of Pseudomonas aeruginosa by rabbit polymorphonuclear leukocytes. Chemotherapy *22*, 203–210.

Nüsslein-Volhard, C., and Dahm, R. (2002). Zebrafish: a practical approach (Oxford University Press).

Olofsson, S.K., and Cars, O. (2007). Optimizing Drug Exposure to Minimize Selection of Antibiotic Resistance. Clin Infect Dis. *45*, S129–S136.

Parks, A.J., Pollastri, M.P., Hahn, M.E., Stanford, E.A., Novikov, O., Franks, D.G., Haigh, S.E., Narasimhan, S., Ashton, T.D., Hopper, T.G., et al. (2014). In silico identification of an aryl hydrocarbon receptor antagonist with biological activity in vitro and in vivo. Mol. Pharmacol. *86*, 593–608.

Pfaffl, M.W. (2001). A new mathematical model for relative quantification in real-time RT-PCR. Nucleic Acids Res. *29*, e45.

Pohjanvirta, R. (2011). The AH receptor in biology and toxicology (Wiley).

Poland, A., and Knutson, J.C. (1982). 2,3,7,8-tetrachlorodibenzo-*p*-dioxin and related halogenated aromatic hydrocarbons: examination of the mechanism of toxicity. Annu. Rev. Pharmacol. Toxicol. *22*, 517–554.

Poland, A., Glover, E., and Kende, A.S. (1976). Stereospecific, high affinity binding of 2,3,7,8-tetrachlorodibenzo-p-dioxin by hepatic cytosol. Evidence that the binding species is receptor for induction of aryl hydrocarbon hydroxylase. J. Biol. Chem. *251*, 4936–4946.

Prasch, A.L., Teraoka, H., Carney, S.A., Dong, W., Hiraga, T., Stegeman, J.J., Heideman, W., and Peterson, R.E. (2003). Aryl Hydrocarbon Receptor 2 Mediates 2,3,7,8-Tetrachlorodibenzo-p-dioxin Developmental Toxicity in Zebrafish. Toxicol Sci. *76*, 138–150.

Queval, C.J., Song, O.-R., Carralot, J.-P., Saliou, J.-M., Bongiovanni, A., Deloison, G., Deboosère, N., Jouny, S., Iantomasi, R., Delorme, V., et al. (2017). Mycobacterium tuberculosis Controls Phagosomal Acidification by Targeting CISH-Mediated Signaling. Cell Rep. *20*, 3188–3198.

Rangel Moreno, J., Estrada García, I., De La Luz García Hernández, M., Aguilar Leon, D., Marquez, R., and Hernández Pando, R. (2002). The role of prostaglandin E2 in the immunopathogenesis of experimental pulmonary tuberculosis. Immunology *106*, 257–266.

Roper, C., and Tanguay, R.L. (2018). Zebrafish as a Model for Developmental Biology and Toxicology. Handbook of Developmental Neurotoxicology (Academic Press), pp. 143–151.

Rowland, M., and Tozer, T.N. (2011). Clinical Pharmacokinetics and Pharmacodynamics Concepts and Applications, Fourth Edition (Lippincott William & Wilkins).

Seidel, S.A.I., Dijkman, P.M., Lea, W.A., van den Bogaart, G., Jerabek-Willemsen, M., Lazic, A., Joseph, J.S., Srinivasan, P., Baaske, P., Simeonov, A., et al. (2013). Microscale thermophoresis quantifies biomolecular interactions under previously challenging conditions. Methods *59*, 301–315.

Smith, S.H., Jayawickreme, C., Rickard, D.J., Nicodeme, E., Bui, T., Simmons, C., Coquery, C.M., Neil, J., Pryor, W.M., Mayhew, D., et al. (2017). Tapinarof Is a Natural AhR Agonist that Resolves Skin Inflammation in Mice and Humans. J. Invest. Dermatol. *137*, 2110–2119.

Solis, N.V., Swidergall, M., Bruno, V.M., Gaffen, S.L., and Filler, S.G. (2017). The Aryl Hydrocarbon Receptor Governs Epithelial Cell Invasion during Oropharyngeal Candidiasis. MBio *8*, e00025-17.

Stedman, R.L. (1968). The chemical composition of tobacco and tobacco smoke. Chem. Rev. *68*, 153–207.

Stockinger, B., Di Meglio, P., Gialitakis, M., and Duarte, J.H. (2014). The aryl hydrocarbon receptor: multitasking in the immune system. Annu. Rev. Immunol. *32*, 403–432.

Takaki, K., Davis, J.M., Winglee, K., and Ramakrishnan, L. (2013). Evaluation of the pathogenesis and treatment of Mycobacterium marinum infection in zebrafish. Nat. Protoc. *8*, 1114–1124.

Uchida, D., Yamashita, M., Kitano, T., and Iguchi, T. (2002). Oocyte apoptosis during the transition from ovary-like tissue to testes during sex differentiation of juvenile zebrafish. J. Exp. Biol. *205*, 711–718.

Van Leeuwen, L.M., Van Der Sar, A.M., and Bitter, W. (2015). Animal Models of Tuberculosis: Zebrafish. Cold Spring Harbor perspectives in medicine *5*, a018580.

Wiegand, I., Hilpert, K., and Hancock, R.E.W. (2008). Agar and broth dilution methods to determine the minimal inhibitory concentration (MIC) of antimicrobial substances. Nat. Protoc. *3*, 163–175.

Wincent, E., Bengtsson, J., Mohammadi Bardbori, A., Alsberg, T., Luecke, S., Rannug, U., and Rannug, A. (2012). Inhibition of cytochrome P4501-dependent clearance of the endogenous agonist FICZ as a mechanism for activation of the aryl hydrocarbon receptor. Proc. Natl. Acad. Sci. USA *109*, 4479–4484.

World Health Organization (2016). WHO treatment guidelines for drug-resistant tuberculosis (World Health Organization), WHO/HTM/TB/2016.04.

World Health Organization (2017). Guidelines for treatment of drug-susceptible tuberculosis and patient care (World Health Organization).

World Health Organization (2019). Global tuberculosis report 2019 (World Health Organization).

Wu, D., Potluri, N., Lu, J., Kim, Y., and Rastinejad, F. (2015). Structural integration in hypoxia-inducible factors. Nature *524*, 303–308.

Yen, Y.-F., Yen, M.-Y., Lin, Y.-S., Lin, Y.-P., Shih, H.-C., Li, L.-H., Chou, P., and Deng, C.-Y. (2014). Smoking increases risk of recurrence after successful anti-tuberculosis treatment: a population-based study. Int. J. Tuberc. Lung Dis. *18*, 492–498.

Yeste, A., Nadeau, M., Burns, E.J., Weiner, H.L., and Quintana, F.J. (2012). Nanoparticle-mediated codelivery of myelin antigen and a tolerogenic small molecule suppresses experimental autoimmune encephalomyelitis. Proc. Natl. Acad. Sci. USA *109*, 11270–11275.

Yeste, A., Takenaka, M.C., Mascanfroni, I.D., Nadeau, M., Kenison, J.E., Patel, B., Tukpah, A.-M., Babon, J.A.B., DeNicola, M., Kent, S.C., et al. (2016). Tolerogenic nanoparticles inhibit T cell-mediated autoimmunity through SOCS2. Sci. Signal. *9*, ra61.

Zelante, T., Iannitti, R.G., Cunha, C., De Luca, A., Giovannini, G., Pieraccini, G., Zecchi, R., D'Angelo, C., Massi-Benedetti, C., Fallarino, F., et al. (2013). Tryptophan catabolites from microbiota engage aryl hydrocarbon receptor and balance mucosal reactivity via interleukin-22. Immunity *39*, 372–385.

Zhong, H., and Lin, S. (2011). Chemical Screening with Zebrafish Embryos. In Methods in molecular biology (Humana Press), pp. 193–205.

STAR★METHODS

KEY RESOURCES TABLE

REAGENT or RESOURCE	SOURCE	IDENTIFIER
Bacterial and Virus Strains		
BL1(DE3) Competent *Escherichia coli*	New England Biolabs	Cat#C2527I
Mycobacterium tuberculosis strain H37Rv	ATCC	ATCC 27294
Mycobacterium tuberculosis strain H37Rv-GFP	Lab collection; *Mtb* H37Rv strain expressing GFP with kanamycin resistance marker	N/A
Mycobacterium tuberculosis RIF-monoresistant patient isolate	Forschungszentrum Borstel	NRZ (FZB-DIAM):18000790
Mycobacterium tuberculosis drug-sensitive patient isolate	Forschungszentrum Borstel	NRZ (FZB-DIAM):18000880
Mycobacterium marinum strain E11	Lab collection	NCBI: txid1131442
Mycobacterium marinum strain M	ATCC	ATCC BAA-535™
Mycobacterium marinum strain M-Wasabi	Lab collection; Takaki et al., 2013	N/A
Chemicals, Peptides, and Recombinant Proteins		
2,3,7,8-Tetrachlorodibenzo-*p*-dioxin (TCDD)	LGC Standards	Cat#CIL-ED-901-C; CAS#1746-01-6
2-Hydroxy-3-methyl-1,4-naphthoquinone (Pht)	Sigma-Aldrich	Cat#S970840
2-Mercaptoethanol	Sigma-Aldrich	Cat#M6250; CAS#60-24-2
2-Methyl-N-[2-methyl-4-[(2-methylphenyl)diazenyl] phenyl]pyrazole-3-carboxamide (CH-223191)	Sigma-Aldrich	Cat#C8124; CAS#301326-22-7
3-Aminobenzoic acid (Tricaine; MS-222)	Sigma-Aldrich	Cat#127671; CAS#99-05-8
4-Aminosalicylic acid	Sigma-Aldrich	Cat#A79604; CAS#65-49-6
25-O-Deacetylrifabutin (LM565)	Toronto Research Chemicals	Cat#D198980; CAS#100324-63-8
AlamarBlue	Thermo Fisher Scientific	Cat#DAL1025
Amikacin	Sigma-Aldrich	Cat#1019508; CAS#37517-28-5
Bedaquiline (TMC-207)	AdooQ Bioscience	Cat#A12327-5; CAS#843663-66-1
CellEvent Caspase-3/7 Green Detection Reagent	Thermo Fisher Scientific	Cat#C10423
Clofazimine	Sigma-Aldrich	Cat#C8895; CAS# 2030-63-9
Complete Protein Inhibitor Cocktail	Roche	Cat#CO-RO
Dicoumarol	Sigma-Aldrich	Cat#287897; CAS#66-76-2
Enrofloxacin	Sigma-Aldrich	Cat#17849; CAS#93106-60-6
Ethambutol	Sigma-Aldrich	Cat#E4630; CAS#1070-11-7
Ethionamide	Sigma-Aldrich	Cat#E6005; CAS#536-33-4
Ethoxyresorufin	Sigma-Aldrich	Cat#E3763; CAS#5725-91-7
Hoechst 33342	Thermo Fisher Scientific	Cat#62249
Hygromycin	Sigma-Aldrich	Cat#H3274; CAS#31282-04-9
Isoniazid	Sigma-Aldrich	Cat#I3377; CAS#54-85-3
Kanamycin	Sigma-Aldrich	Cat#60615; CAS#70560-51-9
Linezolid	Sigma-Aldrich	Cat#PZ0014; CAS#165800-03-3
Live Cell Imaging Solution	Thermo Fisher Scientific	Cat#A14291DJ
Moxifloxacin	Sigma-Aldrich	Cat#32477; CAS#186826-86-8
NucRed Live 647 ReadyProbes™ Reagent	Thermo Fisher Scientific	Cat#R37106
Polyvinylpyrrolidone, avg. mol wt. 40,000 (PVP40)	Sigma-Aldrich	Cat#PVP40 CAS#9003-39-8
Phorbol 12-myristate 13-acetate (PMA)	Sigma-Aldrich	Cat#524400; CAS#16561-29-8
pHrodo Red Zymosan Bioparticles™ Conjugate	Thermo Fisher Scientific	Cat#P35364
Pronase	Sigma-Aldrich	Cat#PRON-RO

(*Continued on next page*)

Continued

REAGENT or RESOURCE	SOURCE	IDENTIFIER
Puromycin	Sigma-Aldrich	Cat#P9620; CAS# 58-58-2
Pyrazinamide	Sigma-Aldrich	Cat#P4050000; CAS#98-96-4
Reporter Lysis Buffer	Promega	Cat#E4030
Rifabutin	Carbosynth	Cat#AR27727; CAS#72559-06-9
Rifampicin	Sigma-Aldrich	Cat#R3501; CAS#13292-46-1
Rifapentine	Sigma-Aldrich	Cat#R0533; CAS#61379-65-5
Streptomycin	Sigma-Aldrich	Cat#S6501; CAS#3810-74-0
SYBR green	Thermo Fisher Scientific	Cat#A25743
Thiacetazone	Santa Cruz Biotechnology	Cat#sc-358574; CAS#104-06-3
Critical Commercial Assays		
Cytotoxicity Detection Kit (LDH)	Roche	Cat#11644793001
iScript cDNA Synthesis Kit	Bio-Rad	Cat#1708891
Luciferase Assay System	Promega	Cat#E1501
Pierce Coomassie Plus (Bradford) Assay Kit	Thermo Fisher Scientific	Cat#23236
RNeasy Mini Kit	QIAGEN	Cat#74106
Experimental Models: Cell Lines		
Hepa-1c1c7	ATCC	RRID: CVCL_0328; CRL-2026
THP-1	ATCC	RRID: CVCL_0006; TIB-202
THP-1 AhR reporter	Moura-Alves et al., 2014	N/A
THP-1 AhR knockdown	Moura-Alves et al., 2014	N/A
HepaRG	Biopredic International	HPR101
Experimental Models: Organisms/Strains		
Zebrafish (*Danio rerio*) strain AB (wild-type line)	EZRC	ZFIN ID: ZDB-GENO-960809-7
Oligonucleotides		
codon-optimized fragment of human AhR encoding amino acid residues 23–475	This study	N/A
ON-TARGET plus Human AHR (NM_001621) siRNA	Dharmacon	Code L-004990-00-0005
ON-TARGET plus Non-targeting Pool siRNA	Dharmacon	Code D-001810-10-05
Primers used for qRT-PCR, see Table S3	This study	N/A
Recombinant DNA		
pET21b	Novagen	Cat#69741
pET30-EK/LIC-mARNT expression plasmid encoding the murine ARNT	A kind gift from Oliver Daumke, MDC Berlin	N/A
Software and Algorithms		
GraphPad Prism, Version 7.0	GraphPad	RRID: SCR_002798; https://www.graphpad.com/
HCS Studio Cell Analysis Software, Version 6.5.0	Thermo Fisher Scientific	RRID:SCR_016787; https://www.thermofisher.com/de/de/home/life-science/cell-analysis/cellular-imaging/high-content-screening/high-content-screening-instruments/hcs-studio-2.html
LightCycler 480 Software	Roche	RRID:SCR_012155; https://lifescience.roche.com/en_de/products/lightcycler14301-480-software-version-15.html
i-control	Tecan	https://lifesciences.tecan.com/plate_readers/infinite_200_pro?p=tab–3#
Maestro Suite, Version 11.8	Schrödinger	RRID:SCR_016748; https://www.schrodinger.com/maestro
NanoTemper Analysis software	NanoTemper Technologies	https://nanotempertech.com/monolith-mo-control-software/

(*Continued on next page*)

Continued

REAGENT or RESOURCE	SOURCE	IDENTIFIER
Photoshop CS5	Adobe	RRID:SCR_014199; https://www.adobe.com
PyMOL Molecular Graphics System, Version 1.8.4.1	Schrödinger	RRID:SCR_000305; https://pymol.org
Zebrafish Bacterial Load Analyzer software, Version 4	Nezhinsky et al., 2012	N/A

LEAD CONTACT AND MATERIALS AVAILABILITY

Further information and requests for resources and reagents should be directed to and will be fulfilled by the Lead Contact, Pedro Moura-Alves (pedro.mouraalves@ludwig.ox.ac.uk). Plasmids generated in this study will be made available upon request. There are restrictions to the availability of HepaRG cells due to a material transfer agreement with Société Anonyme à Directoire et Conseil de Surveillance (Inserm Transfert SA).

EXPERIMENTAL MODEL AND SUBJECT DETAILS

Bacterial Strains and Maintenance

Mycobacterium tuberculosis (*Mtb*) H37Rv, *Mtb* H37Rv-GFP and *Mtb* patient isolates (RIF-monoresistant isolate 18000790 or drug-sensitive isolate 18000880, Forschungszentrum Borstel, Borstel, Germany) were cultured in Middlebrook 7H9 broth (BD) supplemented with 0.05% Tween 80 (Sigma-Aldrich) and 10% albumin-dextrose-catalase (ADC, BD) at 37°C in an orbital shacking incubator at 100 rpm. *Mtb* H37Rv-GFP was kept with additional 25 μg/mL kanamycin (Sigma-Aldrich). *Mycobacterium marinum* E11 and M strains were cultured in Middlebrook 7H9 broth (BD) supplemented with 0.05% Tween 80 (Sigma-Aldrich) and 10% oleic albumin-dextrose-catalase (OADC, BD) statically at 30°C protected from exposure to light. *M. marinum* M strain expressing pTEC15-Wasabi (*M. marinum*-Wasabi; Takaki et al., 2013) was kept with additional 50 μg/mL hygromycin (Sigma-Aldrich).

Cell Culture and Maintenance

THP-1 cells (CVCL_0006, human monocytes, ATCC TIB-202), THP-1 AhR reporter (Moura-Alves et al., 2014) and THP-1 AhR knockdown (Moura-Alves et al., 2014) cells were grown in RPMI 1640 (GIBCO), supplemented with 10% (v/v) heat-inactivated fetal calf serum (FCS; GIBCO), 1% (v/v) sodium pyruvate (GIBCO), 1% (v/v) L-glutamine (GIBCO), 1% (v/v) non-essential amino acids (MEM NEAA, GIBCO), 1% (v/v) 4-(2-hydroxyethyl)-1-piperazineethanesulfonic acid (HEPES, GIBCO) and 0.05 M 2-mercaptoethanol (GIBCO). Hepa-1c1c7 cells (CVCL_0328, mouse hepatocytes, ATCC CRL-2026) were grown in DMEM (GIBCO) supplemented with 10% (v/v) FCS, 1% (v/v) sodium pyruvate and 1% (v/v) L-glutamine, 1% (v/v) HEPES. Undifferentiated HepaRG cells (human hepatic progenitors, HPR101) were cultured in 710 growth medium containing antibiotics and differentiated using 720 differentiation medium containing antibiotics (all Biopredic International). AhR reporter cells were generated in accordance with the protocols available at the Genetic Perturbation Platform (GPP) of the Broad Institute (https://portals.broadinstitute.org/gpp/public/) as described previously (Moura-Alves et al., 2014). In particular, a replication incompetent VSV-g pseudotyped lentivirus expressing the firefly luciferase gene under transcriptional control of a minimal CMV promoter and tandem repeats of the XRE (Cignal Lenti XRE Reporter) was used for infection of THP-1 cells. A similar protocol was used for the generation of AhR knockdown cells. Reporter cells and knockdown cells were kept with additional 5 μg/mL puromycin (Calbiochem). THP-1 monocytes were differentiated into macrophages by treatment with 200 nM of phorbol 12-myristate 13-acetate (PMA, Sigma-Aldrich) for 4 d and rested in plain medium for another 4 d before further experiments. For CYP1A1 enzymatic activity measurements (EROD; Mohammadi-Bardbori and Mohammadi-Bardbori, 2014), Hepa-1c1c7 cells were kept in DMEM medium without phenol red (GIBCO). HepaRG cells were cultured in 710 growth medium for 2 weeks and subsequently differentiated by switching to 720 differentiation medium for another 2 weeks prior to experiments according to the protocols by Biopredic International. All cells were kept in a humidified incubator (Heratherm, Thermo Fisher Scientific) at 37°C with 5% CO_2. Sex of the cell lines was not a consideration in this study. Cell lines were obtained from authentic stocks (ATCC and Biopredic International). If not specified otherwise in the figure legend, the highest concentration of DMSO used in the experiments did not exceed 1%.

Zebrafish Model

All zebrafish (*Danio rerio*) husbandry and experimental procedures adhered to the international guidelines specified by the EU Animal Protection Directive 2010/63/EU and experiments were approved by, and conducted in accordance with the guidelines of the Landesamt für Gesundheit und Soziales (LaGeSo, Berlin, Germany) and the animal welfare committee of the Max Planck Institute for Infection Biology (MPIIB, Berlin, Germany). Only wildtype AB strain zebrafish (ZDB-GENO-960809-7) were used in this study. Adult zebrafish used to generate embryos were housed in 3.5 L or 8 L tanks (Tecniplast) under the following water conditions: 28°C; conductivity ~500 μS (using Instant Ocean Sea Salt); pH 7.4-7.5. Zebrafish embryos were raised and maintained according

to standard protocols (http://zfin.org). All zebrafish embryos used in this study were euthanized on or before 5 dpf. At these ages, sex is indeterminate (Uchida et al., 2002; Liew and Orbán, 2014), hence no distinction between male and female was made.

Zebrafish embryos were maintained in E3 medium (5 mM NaCl, 0.17 mM KCl, 0.33 mM $CaCl_2$, 0.33 mM $MgSO_4$; Nüsslein-Volhard and Dahm, 2002) incubated at 28.5°C in Petri dishes at a maximum density of 50 embryos per dish. To suppress fungal growth, methylene blue (2 mL of 0.1% methylene blue in 1l E3 medium) was added in experiments that did not involve microscopy. Embryos were manually dechorionated at 1 dpf aided by a stereomicroscope (MZ6, Leica). Prior to experimental manipulations, zebrafish embryos were anesthetized using buffered 3-aminobenzoic acid (Tricaine, MS-222, Sigma-Aldrich) at a final concentration of 200 μg/mL. For experiments, embryos were pooled and randomly allocated to experimental groups. At the end of experiments, embryos were euthanized using an overdose of 300 mg/l Tricaine (Sigma-Aldrich).

METHOD DETAILS

Gene Expression Analysis by qRT-PCR

For the isolation of total RNA from cells, buffer RLT (QIAGEN) containing 1% 2-Mercaptoethanol (Sigma-Aldrich) was used. For the isolation of total RNA from zebrafish embryos TRIzol (Invitrogen) was used. RNA extraction was performed using RNeasy Plus Mini kit (QIAGEN) according to the manufacturer's instructions. RNA quality and concentration were determined by spectrophotometry (Nanodrop 2000c, Thermo Fisher Scientific). Complementary DNA (cDNA) was generated using iScript cDNA synthesis kit (Biorad) according to the manufacturer's instructions. Quantitative real time polymerase chain reaction (qRT-PCR) was performed using Power SYBR green (Thermo Fisher Scientific) in a LightCycler® 480 II PCR platform (Roche) running with LightCycler® 480 Software (SCR_012155, Version 1.5.1, Roche). The average threshold cycle of triplicate reactions was applied for all calculations and ΔΔCt method was used (Pfaffl, 2001). Gene expression was normalized to glyceraldehyde-3-phosphate dehydrogenase (*GAPDH*) or β-actin for human and zebrafish samples, respectively. qRT-PCR data were generated from independent experiments, with at least 3 biological replicates per experiment. Sequences of all primers used are listed in Table S3.

Luciferase Reporter Assay

AhR reporter cells were stimulated as depicted in figure legends. For competition assays, AhR reporter cells were pre-incubated with TB drugs for 1 h prior to stimulation with 50 μM Pht. After stimulation, cells were washed using sterile Dulbecco's phosphate-buffered saline (DPBS, GIBCO) and subsequently lysed using 1x concentrated Reporter Lysis Buffer (Promega). Cell lysates were used to determine luciferase activity by Luciferase Assay System (Promega) according to the manufacturer's instructions and luminescence was measured with an Infinite M200 pro reader platform (TECAN). Luciferase activity was normalized to the protein concentration measured by Bradford reaction (Pierce™ Coomassie Plus Assay, Thermo Fisher Scientific). Results are shown as log2 fold induction normalized to the solvent control of the respective time point.

siRNA Knockdown of AhR

THP-1 AhR reporter cells were treated with ON-TARGET plus siRNA AHR or ON-TARGETplus Non-targeting Pool (Dharmacon) for 24 h prior to stimulation with RFB, according to manufacturer's instructions.

EROD Activity *In Vitro*

CYP1A1 is under transcriptional control of AhR (Nebert, Goujon and Gielen, 1972; Poland, Glover and Kende, 1976; Poland and Knutson, 1982). The EROD assay measures the conversion of non-fluorescent ethoxyresorufin by CYP1A1 to the fluorescent product resorufin, where the amount of resorufin-fluorescence is proportional to the enzymatic activity of CYP1A1 (Mohammadi-Bardbori and Mohammadi-Bardbori, 2014). Cells were stimulated as depicted in the figures. After stimulation, cells were washed once using sterile DPBS (GIBCO) and 5 μM ethoxyresorufin (EROD, Sigma-Aldrich) and 10 μM dicoumarol (Sigma-Aldrich) were added to the cells for 1 h. Subsequently, relative fluorescence of resorufin (excitation 535nm/emission 590nm) was measured either in form of an endpoint assay or as kinetic (kinetic reads every 30 min at 37°C, 5% CO_2) using an Infinite M200 pro reader platform (TECAN). EROD activity was corrected to the protein concentration measured by Bradford reaction (Pierce™ Coomassie Plus Assay, Thermo Fisher Scientific) and normalized to the solvent control of the respective time point for end point assay. Endpoint assays are shown as Log2 activity fold induction ans kinetic measurements are shown as total well fluorescence over time.

LDH Release Assay

Release of lactate dehydrogenase (LDH) was quantified using the Cytotoxicity Detection Kit PLUS (Roche) according to the manufacturer's instructions. The percentage of cytotoxicity was calculated as:

$$\text{Cytotoxicity}(\%) = \frac{\text{exp erimental value} - \text{low control}}{\text{high control} - \text{low control}} \times 100$$

Caspase-3/7 Activity Assay

Caspase activity was measured using the CellEvent™ Caspase-3/7 Green Detection Reagent (Thermo Fisher Scientific) according to the manufacturer's instructions. In particular, after stimulation cell nuclei were labeled using NucRed™ Live 647 ReadyProbes™

Reagent (Thermo Fisher Scientific). Subsequently, cells were incubated with CellEvent™ Caspase-3/7 Green Detection Reagent for 30 min and micrographs were acquired using an ArrayScan™ XTI High Content Analysis Reader (Thermo Fisher Scientific). For subsequent analysis of Caspase-3/7 positive cells, nuclear labeling was used to identify and define cells and green fluorescence signal was used to determine caspase-3/7 positive cells.

In Vitro Infections and Analysis

For *in vitro* infections, *Mtb* H37Rv, *Mtb* H37Rv-GFP or *Mtb* patient isolates were cultured to an optical density at 600nm (OD_{600nm}) of 0.5-0.8 and single-cell suspensions prepared by collecting bacterial culture supernatants after centrifugation at 120 x *g* for 10 min. Bacterial CFU were calculated based on growth curves (OD_{600nm} of 1 equals approximately 2.5×10^7 bacteria/mL). THP-1 macrophages were infected with cell culture medium containing a multiplicity of infection (MOI) of 10 for 4 h. After infection, bacteria not internalized were removed by rigorous washing with sterile DPBS (GIBCO). For counting of CFU, cells were lysed using 0.1% Triton X-100 (Sigma-Aldrich) in 1x DPBS (GIBCO) and serial dilutions were prepared in 0.04% Tween20 (Sigma-Aldrich) in 1x DPBS (GIBCO). Bacterial dilutions were plated on Middlebrook 7H11 agar (BD) plates, sealed with parafilm®M (Merck) and incubated at 37°C for approximately 3 weeks. For the analysis of *Mtb*-GFP infected macrophages, cells were fixed using 4% paraformaldehyde (PFA, Electron Microscopy Sciences) containing 1 μg/mL H33342 fluorescent DNA stain (Hoechst) in 1x DPBS (GIBCO) for 30 min at 4°C and stored overnight in 2% PFA in 1x DPBS (GIBCO) at 4°C. Micrographs were acquired using the ArrayScan™ XTI High Content Analysis Reader (Thermo Fisher Scientific) and analysis was performed using the Cellomics® Compartmental Analysis V4 BioApplication (Thermo Fisher Scientific) of the HCS Studio software (SCR_016787, Thermo Fisher Scientific).

Broth Dilution Assay

To determine the minimal inhibitory concentration (MIC) of RFB in the presence or absence of CH-223191 in axenic mycobacterial cultures, we used the previously established broth dilution method (Wiegand, Hilpert and Hancock, 2008). *Mtb* H37Rv or *M. marinum*-Wasabi were cultured to an OD_{600nm} of 0.5-0.8 and subsequently diluted to an OD_{600nm} of 0.1 in their respective culture media. Cultures were diluted once more 1:50 in the respective culture medium and distributed to 96-well plates with round-bottom (Thermo Fisher Scientific). Bacteria were then incubated with different concentrations of RFB in the presence or absence of 12 μM CH-223191. After 7 d for *Mtb* H37Rv and after 4 d for *M. marinum* cultures, 10μl resazurin dye (alamarBlue™; Thermo Fisher Scientific) was added to each well and incubated overnight. On the next day, supernatants were transferred to 96-well plates with clear flat-bottom and absorbance was measured at 570nm using a GloMax Microplate Reader (Promega). Correction wavelength was acquired at 600nm. MICs were determined by comparing the absorbance to culture negative background controls.

Zymosan-pHrodo Phagocytosis Assays

Zymosan is a protein-carbohydrate complex extracted from the cell wall of the yeast *S. cerevisiae*. We used zymosan conjugated to pHrodo (Thermo Fisher Scientific), a pH-sensitive fluorescent dye that increases its brightness in acidic environments. THP-1 macrophages were pre-stimulated with different compounds as depicted in figure legends. After stimulation, supernatants were removed and cells incubated with 0.5 mg/mL pHrodo Red zymosan A BioParticles conjugate (Thermo Fisher Scientific) in 1 x Live Cell Imaging Solution (Thermo Fisher Scientific) for 2 h. Cells were washed rigorously with 1x DPBS and fixed with 2% PFA containing 1 μg/mL H33342 fluorescent DNA stain (Hoechst) in 1x DPBS (GIBCO) for 30 min at 4°C, protected from exposure to light. Micrographs were acquired using the ArrayScan™ XTI High Content Analysis Reader (Thermo Fisher Scientific) and analysis was performed using the Cellomics® Compartmental Analysis V4 BioApplication (Thermo Fisher Scientific) of the HCS Studio software (SCR_016787, Thermo Fisher Scientific). Results are shown as mean of total pHrodo zymosan fluorescence intensity per cell of a 40 field acquisition area acquired with a 20x objective.

Rifabutin Metabolism

Differentiated HepaRG cells or 2 dpf zebrafish embryos were stimulated with 10μM RFB in the culture medium or zebrafish water, respectively. At different time points, supernatants or fish water were collected and used for analysis by ultra-performance liquid chromatography (UPLC). RFB was extracted by adding chloroform/methanol (2:1). After mixing and centrifugation, the organic lower phase was collected and evaporated in a vacuum concentrator. Dried samples were dissolved in 50% methanol, 0.1% formic acid. Subsequently, the RFB extracts were loaded onto an HSSC18 reversed phase UPLC column. RFB was eluted with a linear gradient of 15% acetonitrile to 90% acetonitrile (containing 0.1% formic acid) over 5 min at 45°C and a flow rate of 0.6 mL/min. Eluted compounds were detected by UV absorbance and by ESI-MS detection. RFB was detected by single ion recording (SIR) of m/z 847.5. The ESI-MS detection was operated in an electrospray positive ion mode with a voltage of 0.8 kV, a cone voltage of 15 V and a probe temperature of 600°C. A full mass spectrum between m/z 100 and m/z 1200 was acquired at a sampling rate of 8.0 points/sec. Quantification of RFB was performed by integration of the UV-absorbance peak at 360nm based on a seven point calibration from 1 pmol to 500 pmol of RFB.

Molecular Modeling

First, the conformational space of RFB and RIF was analyzed with the conformational search tool of Maestro (SCR_016748, Version 11.8, Schroedinger), carried out with standard settings as mixed torsional / low-mode sampling. 122 different conformations were found for RFB and 155 for RIF. RFB, RIF and the AhR-inhibitor CH-223191 were docked into the previous described molecular

monomer model of PasB-hAhR (Moura-Alves et al., 2014), utilizing the induced fit docking method of Maestro (SCR_016748, Version 11.8, Schroedinger). Amine bonds of the ligands were allowed to vary in conformation and the ring conformations were sampled with an energy window of 6 kcal/mol. To allow for more room in the binding pocket, during the induced fit procedure several side chains covering the binding pocket of AhR (RFB: residues H291, F295, C300, M340, M348, F351; RIF: F287, T289, H291, F295, L308, Y322, Y322, I325, C333, M340, M348, F351, L353, V363, S365, I379, V381) were substituted with alanine (trimmed) in the initial docking step. In the second step these trimmed residues were reconstituted and refined together with amino acids located 5.0 Å around the initial ligand pose before the Glide re-docking (third step). The binding energy of the different molecules (ΔG binding) was calculated using the Prime MM-GBSA tool of Maestro (SCR_016748, Version 11.8, Schroedinger). Heterodimer models of hAhR and Arnt each comprising HLH / PasA / PasB domains were generated based on crystal structures on one hand of the homologous Hif2a /ARNT complex (Wu et al., 2015) including dynamic studies thereof (Motta et al., 2018) and on the other hand of the CLOCK/ Bmal1 complex (Huang et al., 2012). Structural images were generated with PyMOL Molecular Graphics System (SCR_000305, Version 1.8.4.1, Schroedinger)

AhR Binding Studies Using MST

A codon-optimized fragment of human AhR encoding amino acid residues 23–475 was commercially synthesized (MWG Eurofins) and cloned into pET21b (Novagen) using NcoI and XhoI restriction sites. The pET30-EK/LIC-mArnt expression plasmid encoding the murine Arnt (residues 85-465) was a kind gift from Oliver Daumke (MDC Berlin). For protein expression, BL21(DE3) cells were co-transformed with both plasmids. Bacteria were grown to OD_{600nm} of 0.6 in LB medium and protein expression was induced with 0.5 mM isopropyl-β-D-thiogalactopyranoside (IPTG), followed by overnight expression at 18°C. Proteins were purified as previously described (Huang et al., 2012). Specifically, cell pellets were resuspended in lysis buffer containing DNaseI (Serva) and Complete Protein Inhibitor Cocktail (Roche) and lysed using a French Press. The clarified lysate was applied onto a HisTALON Superflow column (Clontech) and bound protein was eluted with increasing concentrations ofimidazole. Elution fractions were buffer exchanged and N-terminal 6xHis-tags were removed with PreScission protease overnight at 4°C. Cleaved protein complex was further purified on a HiTrap Heparin HP column (GE Healthcare), followed by SEC on a Superdex 200 10/300 GL equilibrated in 20 mM HEPES pH 8.0, 200 mM NaCl, 5% glycerol, and 5 mM DTT. Peak fractions containing AhR-Arnt were pooled and concentrated using Amicon filter units (Millipore).

Binding studies using purified AhR-Arnt complex were performed by microscale thermophoresis (MST) using the Monolith® NT.LabelFree (NanoTemper Technologies GmbH). MST measurements were performed according to the manufacturer's instructions. In particular, a constant protein concentration of 250 nM diluted in assay buffer including 0.1% Pluronic F-127 was used. To this, a serial dilution of ligand dissolved in DMSO was added. After short incubation, samples were filled into NT LabelFree Zero Background MST Premium coated capillaries (NanoTemper Technologies GmbH). Measurements were carried out at 22°C. MST traces were collected with an LED excitation power of 20% and a MST laser power of 20%–40%. For analyzing the interaction affinity, the dissociation constant (K_d) for each ligand was calculated using the NanoTemper Analysis software by plotting changes in the normalized fluorescence (ΔFnorm [‰]) as a function of the ligand concentration.

Zebrafish Chemical Stimulations

In stimulation experiments, 2 dpf embryos were treated with different compounds in E3 medium for the durations indicated in the respective figures. In experiments using the AhR inhibitor CH-223191 (Sigma-Aldrich), embryos were pre-exposed to 10 μM CH-223191 in E3 for 2 h prior to the experiment and the inhibitor was present during the entire duration of the experiment.

Zebrafish Cyp1a Enzymatic Activity

EROD experiments were conducted as previously described (Nacci et al., 1998). In detail, during the assay non-fluorescent 7-ethoxyresorufin diffuses into the embryo where it is converted by Cyp1a to the fluorescent product resorufin. After compound stimulation or immersion with *M. marinum*, 2 dpf zebrafish embryos were washed and placed in E3 medium containing 0.4 μg/mL of 7-ethoxyresorufin (Cayman Chemical) for 5 min. After incubation, embryos were anesthetized with 200 μg/mL tricaine (MS-222, Sigma-Aldrich) and placed in black 96-well plates with clear bottom (Thermo Fisher Scientific) and micrographs were acquired using the ArrayScan™ XTI High Content Analysis Reader (Thermo Fisher Scientific). Brightfield images were used to identify embryo outlines and embryo fluorescence (filters excitation: 549/15nm, emission: 590-624nm) was determined as a readout of Cyp1a activation using the Cellomics® Zebratox BioApplication (Thermo Scientific) of the HCS Studio software (SCR_016787, Thermo Fisher Scientific).

Zebrafish Toxicity

For the assessment of compound toxicity for zebrafish embryos, brightfield images were acquired using the ArrayScan™ XTI High Content Analysis Reader (Thermo Fisher Scientific). To evaluate toxicity, the Cellomics® Zebratox BioApplication (Thermo Fisher Scientific) of the HCS Studio software (SCR_016787, Thermo Fisher Scientific) was used. Head-to-tail distance and embryo straightness served as measure for compound toxicity.

Zebrafish Infection

In infection by immersion experiments, 2 dpf embryos were placed in E3 medium inoculated with different concentrations of *M. marinum* E11 and incubated at 28°C for time of the experiment. Inoculum preparations and infection by intravenous injection

of zebrafish embryos were performed as described (Benard et al., 2012). In particular, a colony of *M. marinum*-Wasabi was resuspended in 10 mL Middlebrook 7H9 broth (BD) containing 10% ADC (BD), 0.05% Tween 80 (Sigma-Aldrich) and 50 μg/mL hygromycin (Sigma-Aldrich). The culture was set to an OD_{600nm} of 0.2-0.3 and cultured statically overnight at 28°C. On the day of infection, OD was measured again to ensure the logarithmic growth phase of the culture and bacteria were harvested by centrifuging and washing 3 times in sterile 1x PBS. Based on previous growth curves, an OD_{600nm} of 1 corresponded to approximately 10^8 *M. marinum*/mL and was used to determine CFU for infection. Bacteria were centrifuged and resuspended in 2% polyvinylpyrrolidone (PVP40, Sigma-Aldrich) in PBS (w/v) to the desired concentration. Before infection, zebrafish embryos were staged at 28 hpf based on morphological criteria. Anesthesia was induced using 200 μg/mL tricaine (MS-222, Sigma-Aldrich) approximately 10 min prior to infection. Borosilicate glass microcapillaries (Science Products GmbH BF100-78-10, with filament) were loaded with the bacterial inoculum using a microloader tip and subsequently mounted to a micromanipulator (Sutter Instrument, MM-33) with stand (World precision Instruments, M10L magnetic stand). Injections were performed using a FemtoJet microinjector (Eppendorf) under a Leica M50 stereomicroscope (Leica). Anesthetized embryos were positioned on a flat 1% agarose plate and a scale bar was used to determine the desired injection volume of approximately 1 nL/embryo. 200 CFU Wasabi-expressing *M. marinum* were injected into the caudal vein of a single embryo. After infection embryos were rested for 30 min in E3 medium at 28°C.

RFB Treatment of *M. marinum*-Infected Zebrafish

Infected zebrafish embryos were pooled and randomly distributed into different experimental groups. Embryos were incubated in either 10 μM CH-223191 or DMSO at 28°C for 2 h. Subsequently, embryos were treated once with either 5 μM or 10 μM RFB, or with DMSO as untreated control. Treatment was applied by adding RFB directly to the medium. At 4 d post infection (dpi), embryos were anesthetized and imaged using a stereomicroscope (MZ16FA, Leica) equipped with a DFC3000Gdigital color camera (Leica). Brightfield and fluorescence stereomicroscopy overlays were created using Adobe Photoshop (SCR_014199, Photoshop CS5, Adobe). To quantify the amount of fluorescent bacteria, bacterial pixel counts were determined and analyzed using Zebrafish Bacterial Load Analyzer software (Version 4, A. Nezhinsky, University Leiden Institute of Advanced Computer Science, Leiden, the Netherlands).

QUANTIFICATION AND STATISTICAL ANALYSIS

For *in vivo* experiments, zebrafish embryos were randomly assigned to different experimental groups and group size was chosen to allow a significance threshold α of 0.05 with a power of 80% ($\beta = 0.2$). For *in vitro* experiments, cells were randomly distributed in different culture well plate positions. All statistical details of experiments can be found in the figure legends. Data are presented as mean ± SD (for individual experiments) or as mean ± SEM (for pooled experiments), as described in figure legends. To compute P values, unpaired t test or Mann-Whitney test was used, as described in figure legends. GraphPad Prism (SCR_002798, version 7.0, GraphPad) was used for analysis and differences were considered statistically significant at $p \leq 0.05$.

DATA AND CODE AVAILABILITY

This study did not generate any unique datasets or code.